Uncoupled changes in phytoplankton biomass and size structure in the western tropical Atlantic

Gabriel Bittencourt Farias, Juan-Carlos Molinero, Claire Carré, Arnaud Bertrand, Beatrice Bec, Pedro Augusto Mendes De Castro Melo

Journal of Marine Systems
March 2022, Volume 227 Pages 103696 (14p.)
https://doi.org/10.1016/j.jmarsys.2021.103696
https://archimer.ifremer.fr/doc/00741/85331/

Uncoupled changes in phytoplankton biomass and size structure in the western tropical Atlantic

Bittencourt Farias Gabriel [1, *], Molinero Juan-Carlos [2], Carré Claire [2], Bertrand Arnaud [1, 2, 3], Bec Beatrice [2], Mendes De Castro Melo Pedro Augusto [1]

[1] Departamento de Oceanografia, Universidade Federal de Pernambuco, Avenida Arquitetura, S/N, 50670-901 Recife, PE, Brazil
[2] MARBEC, Univ Montpellier, IRD, Ifremer CNRS, Montpellier, France
[3] Universidade Federal Rural de Pernambuco, Departamento de Pesca e Aquicultura, Recife, PE, Brazil

* Corresponding author : Gabriel Bittencourt Farias, email address : bittencourt.bio@gmail.com

Abstract :

Structural changes in phytoplankton communities have large influence on marine elemental cycling, food web dynamics and carbon export. Here we used data from two field expeditions, performed in spring and fall, over a coast-offshore gradient to investigate phytoplankton structure and dynamics in the Southwestern Tropical Atlantic (SWTA). Results revealed a predominant role of the thermohaline structure as the main driver of phytoplankton dynamics regardless the season. In fall, the thermocline and nutricline shallowing promoted a biomass increase, which was 3-fold higher around the oceanic islands. The structure of phytoplankton community mainly varied vertically, with Prochlorococcus pigments contributing greatly to the higher nutrient Deep Chlorophyll Maximum, whereas other Cyanophyceae predominated in nutrient poor surface layers during the two seasons. In addition, a clear coast-offshore variability in the new production (Fp) was observed, with the shelf region displaying higher values (up to 0.21), promoted by larger Bacillariophyceae pigments concentration, thus suggesting a coastal influence on shelf production. Although the phytoplankton biomass increased seasonally, our results highlighted a predominance of recycled production (Fp) and uncoupled dynamics between biomass and size of phytoplankton structure, with pico- and nanophytoplankton dominating the relative biomass, i.e., ca. 80% of the community in both seasons. We hypothesize that these patterns may result from a strong nitrogen limitation (N:P of around 3:1), which likely constrain a pronounced growth of the microphytoplankton.

Graphical abstract

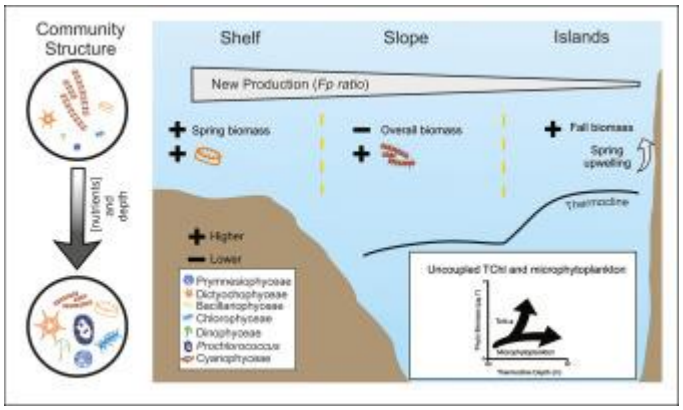

Highlights

► Uncoupled dynamics between phytoplankton size structure and biomass were revealed. ► A decreasing gradient of biomass and new production from shelf to offshore was pointed out. ► Seasonal changes in thermocline shape the phytoplankton dynamics and size structure. ► Phytoplankton diversity increased with depth, but was mainly dominated by small cells.

Keywords : Primary producers dynamics, pigment composition, tropical thermohaline structure, nutrient ratios

1. Introduction

Phytoplankton communities are essential components in marine ecosystems functioning and key players in the global carbon cycling, contributing to about half of Earth primary productivity (Litchman et al., 2015). They encompass a variety of taxonomic and functional entities associated to diverse biogeochemical cycles, and therefore their structural changes alter marine elemental cycling (Finkel et al., 2010; Litchman et al., 2015). Understanding how phytoplankton respond to the environmental variability is thus critical to assess not only changes in biogeochemical cycles, but also their implications in food webs functioning under global change scenarios.

Phytoplankton structure, biomass and growth are shaped by multiscale interlinked environmental forces, from long term, large scale factors, i.e., climate, deep circulation/geostrophic currents, to short term, local ones, i.e., temperature, light, turbulence and nutrients concentration (Jardine et al., 2017; Ryabov et al., 2010; Toseland et al., 2013). The relative importance of these forces however, greatly varies among phytoplankton functional groups due to the diversity of life history traits and ecophysiological requirements (Falkowski and Oliver, 2007; Litchman and Klausmeier, 2008). For instance, nutrient competition favors niche partitioning and shapes phytoplankton distribution, with Cyanophyceae thriving in low nitrogen-to-phosphorus waters over Bacillariophyta that are less efficient phosphorus competitors (Egge, 1998; Vrede et al., 2009). Moreover, empirical evidence on competition theory has shown that light intensity and temperature further influence the minimum nutrient requirements of phytoplankton taxa (Burson et al., 2018; Lewington-Pearce et al., 2019). Hence, a thorough assessment of phytoplankton dynamics requires an integrative multi-scale, multi-stressor approach to effectively quantify, and eventually model, phytoplankton responses under changing ocean conditions.

In the last decade, growing interest has focused on plankton functional traits. Probably the most prominent is body size, as it influences community structure, stability, and food webs trophodynamics (Litchman and Klausmeier, 2008). In oligotrophic systems, smaller phytoplankton groups (picophytoplankton, < 2 μm and nanophytoplankton, 2-20 μm) are known to absorbe nutrients more efficiently than large phytoplankton cells due to their higher surface-volume ratio (Chisholm, 1992; Flombaum et al., 2013; Lange et al., 2018). In contrast, larger cells (microphytoplankton, > 20 μm) are generally dominant under turbulent conditions with higher nutrient concentration (Falkowski and Oliver, 2007). Hence, the contribution of pico- and nanophytoplankton to phytoplankton biomass change along with nutrient gradients and primary productivity (Bell and Kalff, 2001). However, empirical evidence has shown that in oligotrophic ecosystems the increase of phytoplankton biomass may be decoupled from significant variations in the size structure, with a predominance of smaller cells during high productivity events (Dandonneau et al., 2004; Marañón et al., 2003, 2000; Rii et al., 2016).

The southwestern tropical Atlantic (SWTA) is an oligotrophic area characterized by the intrusion of subtropical underwater channeled by the North Brazil Undercurrent - North Brazil Current system (Dossa et al., 2021; Stramma and England, 1999). The thermohaline structure of the region is characterized by the existence of different provinces portrayed by specific thermocline structure and stratification strength (Araujo et al., 2011; Assunção et al., 2020). How such environmental configuration shapes the structure of primary producers remains unclear, although their understanding might shed light on the dynamics of primary producers in oligotrophic oceans regions.

Here, using data from two oceanographic surveys performed during austral spring and fall in the SWTA, we analyzed the space-time variability of phytoplankton biomass

and size structure along a coast-offshore gradient, and quantified the influence of thermohaline stratification on the phytoplankton community. We further test the extent of coupling between phytoplankton biomass and size structure (i.e., whether high biomass is driven by large, coupled production, or small phytoplankton cells, uncoupled production).

2. Material and Methods

2.1. Study area

The SWTA has a narrow continental shelf not exceeding 40 km with a shelf break varying between 40 and 80 meters and a continental slope between 1600 and 3600 m (Knoppers et al., 1999). The region is governed by the western boundary current system, which is dominated by the North Brazilian undercurrent and the North Brazilian current (Fig. 1b) (da Silveira et al., 2000; Dossa et al., 2021). Offshore, the geomorphology is characterized by a chain of seamounts (between 20 and 250 meters high), the Fernando de Noronha ridge that includes the oceanic island of Rocas Atoll and the Fernando de Noronha Archipelago (Fig. 1b) (Castello, 2010; Kikuchi, 2002; Mabesoone and Coutinho, 1970). This area is further influenced by the central and southern branch of the South Equatorial current and the South Equatorial Under current, which form the South Equatorial Current System (Dossa et al., 2021).

Two thermohaline provinces have been defined from the continental slope to the oceanic islands (Fig. 1b) (Assunção et al., 2020). The first area located along the continental slope corresponds to the western boundary current system, which is characterized by a low thermal stratification, the presence of frequent and thick barrier layer and an average mixed layer depth of 53 and 39 m in spring and fall, respectively. The second area encompasses the Rocas Atoll and part of Fernando de Noronha ridge seamounts and corresponds to the South Equatorial Current System. This area is

characterized by a deeper mixed layer (~90 and 46 m in spring and fall, respectively), a sharp thermocline, a strong static stability and weak surface current (~0.34 $m.s^{-1}$). Between these two thermohaline provinces lies a transitional area, with an intermediate stratification and moderate static stability (Fig. 1b).

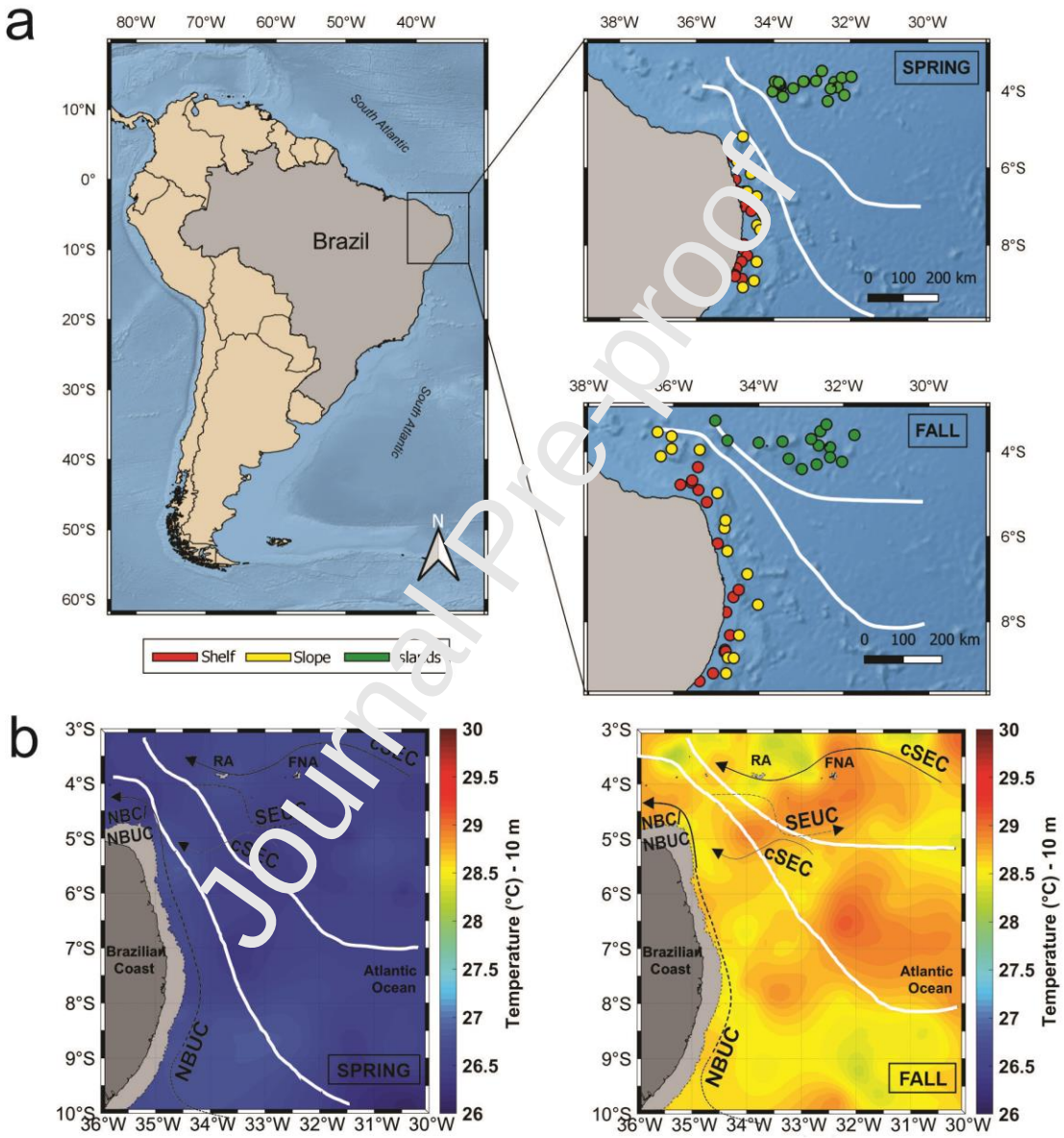

Fig 1. (a) Study area with the position of sampling stations surveyed during austral spring and fall in the three regions, Shelf: red; Slope: yellow; Islands: green. White solid lines show themohaline areas. (b) 10 m depth temperature field in spring and fall. White solid lines delimit thermohaline areas. The continental shelf limited by the isobaths of 60 m is represented in light grey. RA: Rocas Atoll; FNA: Fernando de Noronha archipelago. The main currents are represented. cSEC: central branch of the

South Equatorial Current; SEUC: South Equatorial Undercurrent; NBUC: North Brazil Undercurrent; NBC: North Brazil Current. Redrawn from Assunção et al. (2020).

2.2.Field Collection

Samples were collected during the "Acoustics along the BRAzilian COaSt (ABRACOS)" oceanographic campaigns, carried out in Austral spring (30 August - 20 September of 2015 - ABRAÇOS 1; Bertrand, 2015) and fall (9 April - 9 May of 2017 - ABRAÇOS 2; Bertrand, 2017) on board the French R/V ANTEA. Spring 2015 and fall 2017 are representative of canonical spring and fall conditions in terms of thermohaline structure and currents dynamics (Assunção et al., 2020; Dossa et al., 2021). Hence, hereafter we will only use spring and fall to identify the oceanographic campaigns. ABRACOS 1 comprehended 54 stations encompassing the shelf, the continental slope and oceanic islands (Fig. 1a), while ABRACOS 2 extended the study area towards the western part of the Fernando de Noronha ridge and totaled 61 stations (Fig. 1a). In all stations, vertical profiles of conductivity, temperature, depth and fluorescence were acquired from the surface to 1000 m depth (or 10 m above the sea bottom) using a CTD Seabird SBE911+.

Water sampling for pigments and nutrients were carried out using a rosette at four depths defined by CTD profiles: Surface, Mixed Layer, Deep Chlorophyll Maximum (DCM) (which showed a mean depth of 100 m in spring and 80 m in fall) and at 200 m. In shelf shallow stations (< 50 m depth), where no peak of fluorescence was observed, the DCM and 200 m samplings were replaced by a Shallow Bottom, sampling at ~10 m above the bottom. For each station and sampled depth, 500 ml of water were filtered in Whatman GF/F glass fiber for the estimation of pigment concentrations of the total phytoplankton community. Size fractionation of water samples was done using a 20 µm filter meshes to estimate the biomass of pico- and

nanophytoplankton (< 20 µm) and microphytoplankton (> 20 µm, by the difference between total and < 20 µm fractions). Filters were stored at -80ºC for subsequent HPLC pigment analysis.

Water samples for nutrient concentrations estimation (NOx [NO_2^- + NO_3^-], PO_4^{3-} and SiO_4^{4-}) were collected in 30 ml falcon tubes, pasteurized (heated at 80°C for 2.5 hours in an oven) and frozen to ensure stability until the laboratory analysis. Nutrient analyses were achieved using classical colorimetric methods (Grasshoff et al., 1983).

2.3.*HPLC analyses*

Chemotaxonomic analysis was carried out on an Agilent Technology 1200 series HPLC following the LOV Method described in Hooker et al. (2000), to assess phytoplankton biomass and diversity. Pigments were extracted in 100% methanol in the dark for 5 minutes at 4ºC. Samples were then sonicated and filtered on cellulose acetate filters to remove cell debris. A 600 µl aliquot was diluted with 150 µl Milli-Q water. For the analysis, 125 µl of this solution was taken and diluted in an injection loop with 125 µl of a 28 mM solution of Tetrabutyl ammonium acetate. The pigments were then separated on a ZORBAX Eclipse XDB-C8 column from Agilent Technology, with 3 mm in diameter, 150 mm in length and 3.5 µm in porosity. The column temperature was maintained at 60°C and the flow rate at 0.55 ml min^{-1}. The separation was based on a linear gradient between a solution of methanol/Tetrabutyl ammonium acetate 28 mM, 70:30 (v/v), and a 100% solution of methanol. Chlorophyll-a + Divinyl Chlorophyll-a were used to determine total phytoplankton biomass (TChl-a), while all other pigment markers allowed identifying major algal groups (Table 1). The HPLC system was calibrated with external standards (DHI Water and Environment, Horsholm, Denmark).

Taxa	Pigments	Acronym
Dictyochophyceae	19′Butanoyloxyfucoxanthin	19BF
Bacillariophyceae	Chlorophyll$_{C3}$,Chlorophyll$_{C2}$, Diatoxanthin, Fucoxanthin	Chl$_{C2}$, Chl$_{C3}$, dia, fuco
Prymnesiophyceae	19′Hexanoyloxyfucoxanthin	19HF
Cryptophyceae	Alloxanthin	allo
Dinophyceae	Diatoxanthin, Peridin	dia, peri
Chlorophyceae	Chlorophyll-*b*, Neoxanthin, Violaxanthin	Chl-*b*, neo, vio
Prochlorococcus	Divinyl Chlorophyll-*b*	div Chl-*b*
Cyanophyceae	Zeaxanthin	zea
All community (TChl-a)	Chlorophyll-*a*, Divinyl Chlorophyll-*a*	Chl-*a*, div Chl-*a*

Table 1. Pigment biomarkers in major phytoplankton groups. Selected following Roy et al. (2011).

2.4.Data analysis

The overall methodological approach is described in the Figure 2. Average stations values of biological and environmental variables for each region and depth were calculated to generate mean vertical profiles (Fig. 3) The biological (TChl-a, see Table 1) and environmental (nutrients, temperature and salinity) data were tested for normality (Kolmogorov-Smirnov) and homoscedasticity (Levene). Subsequently, these data were used for comparison among seasons (spring and fall) and diel periods (day and night) using t-test or Mann-Whitney (MW), and by depth (Surface, Mixed Layer, Shallow Bottom, DCM and 200 m) and region (shelf, continental slope and islands) using parametric (one-way ANOVA) or non-parametric (Kruskal-Wallis, KW) analysis of variance (Fig. 2), depending on the normality of the data. Day and night samples were aggregated since no significant differences were found among them (see Supplementary Figure 1).

To examine the variability in phytoplankton communities, we applied a PERMANOVA in log-transformed biological data using a Bray Curtis similarity matrix with the software *PRIMER 6* (Clarke and Gorley, 2006) (Fig. 2). Additionally, to

evaluate nonlinear interactions between environmental factors and phytoplankton biomass, we used Generalized Additive Models (GAMs) (Fig. 2). GAMs allow one response variable to be fitted by several predictors in additive models and have the advantage of not requiring an *a priori* specification of functional relationships, which is suitable for describing complex ecological interactions. The model assumes that the effects of each predictor on the response variable can be described by smooth functions (Hastie and Tibshirani 1986; Wood 2006). Here, we modeled the response of phytoplankton taxa and TChl-a, as a proxy for phytoplankton community, to the effect of nutrients, physical (salinity, mixed layer depth and barrier layer thickness) and spatial (depth and regions) factors, using the function 'gam' in the R package 'mgcv' (Wood, 2011). Models did not include outliers and we used the Generalized cross-validation (GCV) score for model selection. GAMs were constructed using the R package 'mgcv' (Wood 2011).

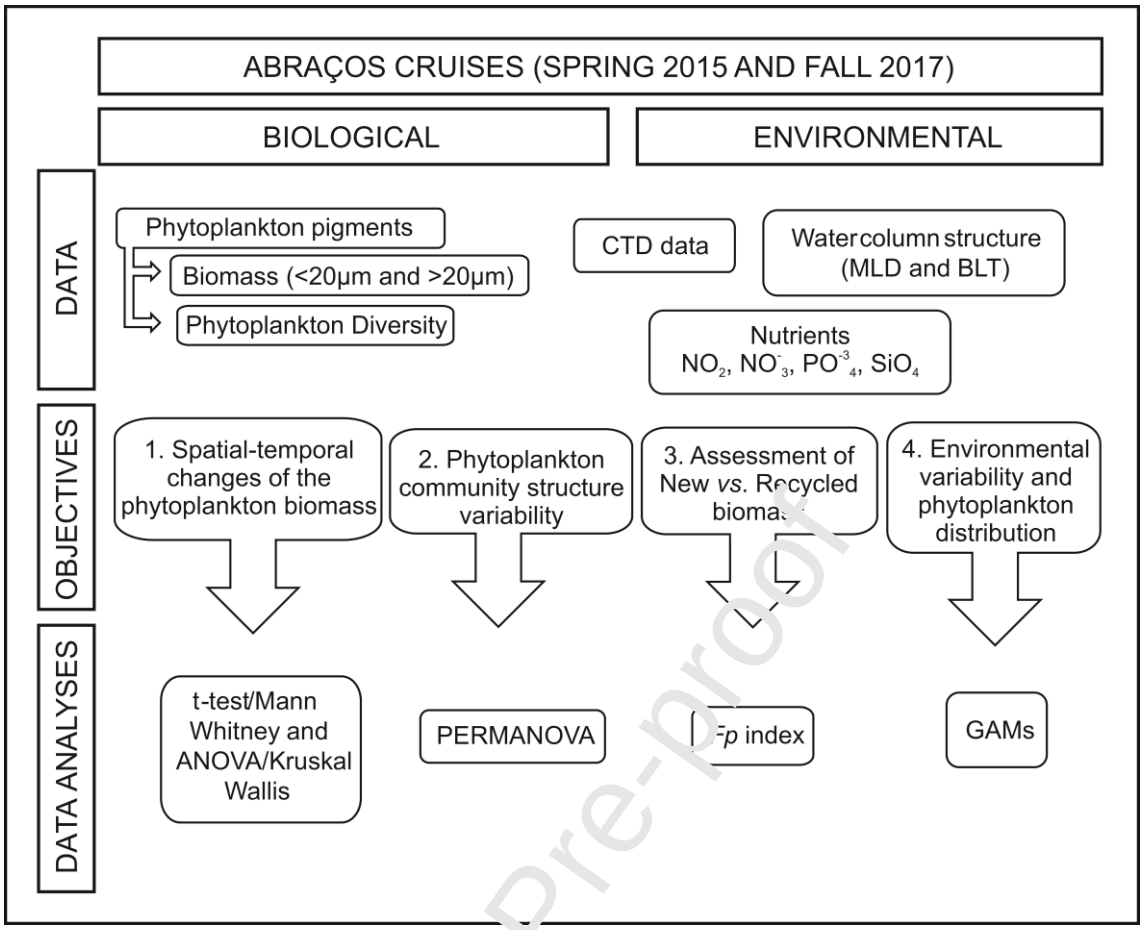

Fig 2. Flow diagram of the research procedure of data collection and analysis. MLD: mixed layer depth; BLT: barrier layer thickness.

The phytoplankton size structure can also be inferred from the trophic status of producer communities. This was assessed by the quantification of the *Fp* index *sensu* Claustre (1994) (Fig. 2). The *Fp* index denotes the biomass ratio of the phytoplankton involved in the new production over the total phytoplankton:

$$Fp = \frac{\sum \text{fuco} + \sum \text{peri}}{\sum \text{fuco} + \sum \text{peri} + \sum \text{19'-HF} + \sum \text{19'-BF} + \sum \text{zea} + \sum \text{Chl b} + \sum \text{allo}}$$

where the numerator corresponds to the new production composed by Dinophyceae and Bacillariophyceae, and the denominator corresponds to the total biomass of the main

groups of the phytoplankton community. To search for seasonal variabilities in the *Fp* values we used t-test or Mann-Whitney, depending on the normality of the data.

For all analysis, p values < 0.05 were considered significant.

3. Results

3.1. Environmental seascape

Sea surface temperature was higher in fall than spring (28.9 ºC vs. 26ºC; t-test, $p < 0.001$) regardless the region (Fig 1b). In the shelf region, temperature was homogeneous along the vertical gradient (~26ºC and 28ºC in spring and fall, respectively), while in the continental slope and islands stations the thermal vertical structure showed a general decrease along with depth, with temperature values at DCM varying between seasons (~23ºC and ~25ºC in spring and fall, respectively). Likewise, in the 200 m depth temperature was higher (from ~18ºC to 15 C in spring and fall, respectively) in the continental slope (MW test, $p < 0.001$) than in the islands stations, where it remained constant among seasons (~12.5ºC) (Fig. 3a; Supplementary Table 1).

Salinity varied between 35 and 37 and showed a slight surface coast-offshore gradient with lower values observed in islands stations (ANOVA, $p < 0.001$), with an average of 36.2, in spring, and 35.9 in fall. The vertical profiles showed that DCM and 200 m depth were characterized by higher salinities over the continental slope in both seasons (t-test, $p < 0.001$), with average values of 37.02 at the DCM and 36.06 at 200 m depth in spring, and 37.17 at the DMC and 35.57 at 200m in fall (Fig. 3a; Supplementary Table 1).

Regardless the season, shelf stations showed a slight vertical increase of nutrients concentration, whereas stations of the continental slope and islands displayed an increased gradient of PO_4^{3}, SiO_4^{-4}, and NO_3^{-}, with a depleted surface layer (Surface

and Mixed Layer) separated from a richer deeper layer (DCM and 200 m depth) (Fig. 3b and c; Supplementary Table 1). Overall, the average nutrient concentration was higher in fall (Supplementary Table 1), except for the average NO_3^- (3.58 *vs.* 0.71 µmol l^{-1}) and SiO_4^{-4} (1.59 *vs.* 1.26 µmol l^{-1}) concentrations at the DCM (Fig. 3c; Supplementary Table 1). In spring, SiO_4^{-4} surface concentrations were higher in the shelf than offshore (KW test, p= 0.003; ~0.84 µmol l^{-1}), with some stations reaching ~1.5 µmol l^{-1}, whereas the islands stations showed higher surface PO_4^{3-} (ANOVA, p= 0.002; ~0.10 µmol l^{-1}) (Fig. 3c; Supplementary Table 1). The continental slope showed slightly higher surface NO_3^- in both seasons (Surface and Mixed Layer; ~ 0.07 and 0.32 µmol l^{-1} in spring and fall respectively), although no statistical difference was found between regions. At the DCM, nutrients concentration was higher in the islands stations at both seasons (MW test, p< 0.05) (Fig 3b and c; Supplementary Table 1).

An evident increase with depth in NO_2^- concentration was observed during fall in the shelf, with a NO_2^- depleted surface (0.006 µmol l^{-1}) and a richer layer in Shallow Bottom (0.021 µmol l^{-1}) (Fig. 3b; Supplementary Table 1). This feature was conspicuous in the continental slope and islands showing a well-defined primary nitrite maximum with a NO_2^- enrichment near the DCM. This was more evident in fall (0.02 µmol l^{-1} *vs.* 0.08 µmol l^{-1} in the continental slope and 0.05 µmol l^{-1} *vs.* 0.07 µmol l^{-1} in the islands), although the NO_2^- concentrations were statistically different only in the continental slope (MW, p= 0.008).

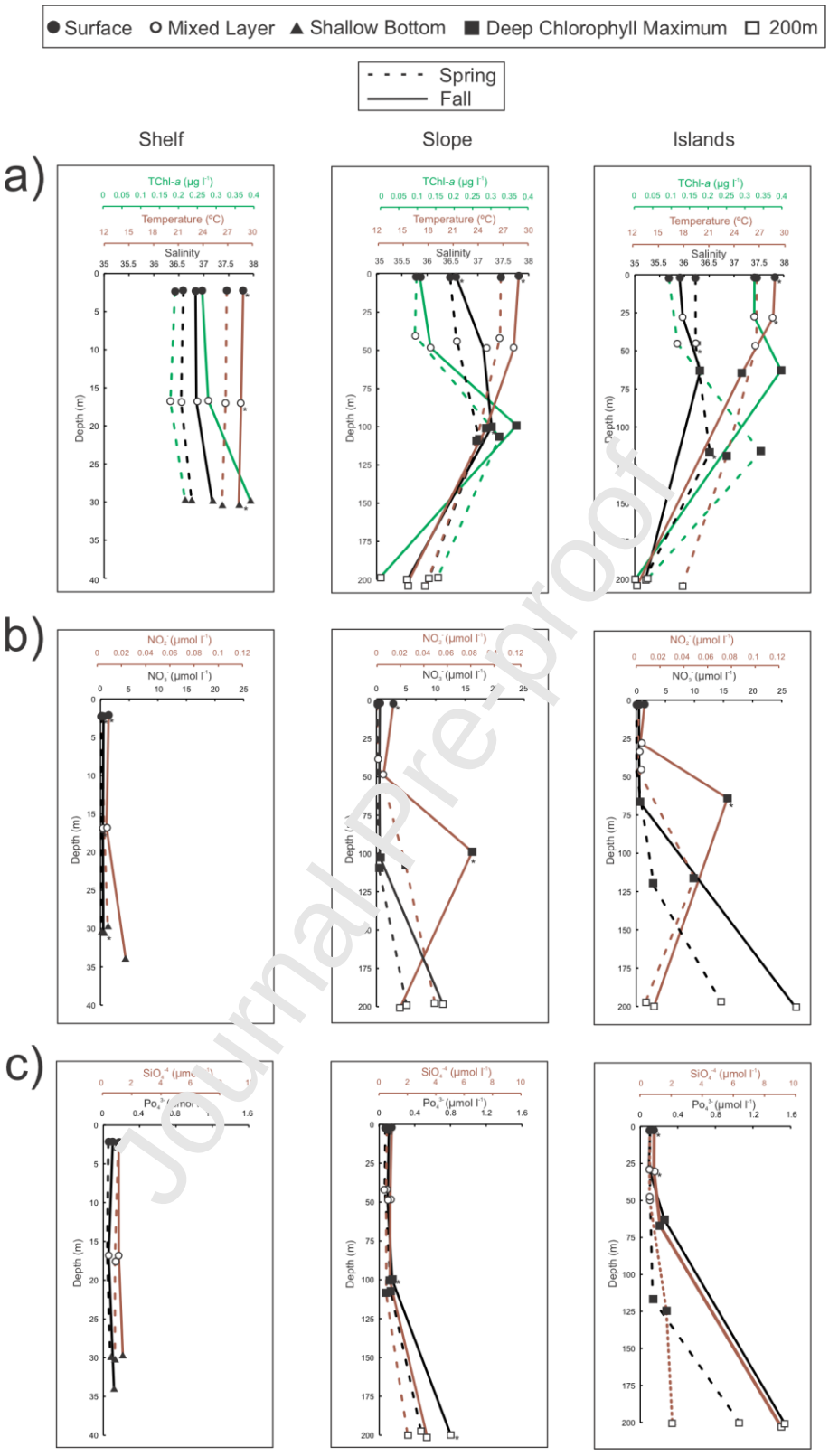

Fig 3. Vertical profiles of average values of temperature, salinity, TChl-a and nutrients at the depths sampled by the rosette in spring (dotted line) and fall (continuous line). The symbol * denotes depths at which the concentrations were statistically different between seasons. Notice different depth scales in the shelf. (a) average TChl-a, temperature and salinity; (b) average concentrations of NO_2 and NO_3^-; (c) average concentrations PO_4^{3-} and SiO_4^{4-}.

3.2. *Phytoplankton biomass*

The total Chl-a (TChl-a: Chl-a + divinyl Chl-a) concentration ranged from 0.01 to 0.49 (μg l^{-1}) in spring, and 0.003 to 1.7 μg l^{-1} in fall. Overall, TChl-a was higher in fall, but this difference was only significant around the islands (MW test; $p < 0.05$), where it displayed a threefold increase in biomass on the surface layer (Fig 4; Supplementary Table 1). In spring, the shelf stations showed higher TChl-a in the surface layer (Surface and Mixed Layer; KW test, $p < 0.5$; ~ 0.18 μg l^{-1}), while the continental slope and islands stations showed similar concentrations (Surface and Mixed Layer, ~ 0.10 μg l^{-1}). In the shelf region, Shallow Bottom TChl-a values were 0.22 and 0.39 μg l^{-1} on spring and fall, respectively, with some stations showing concentrations similar to the DCM. During fall, islands stations displayed higher TChl-a than the other regions in the surface layer (Surface and Mixed Layer; KW test, $p < 0.001$; ~0.32 μg l^{-1}), whereas in DCM islands and continental slope showed similar TChl-a in both seasons (~0.34 and ~0.39 μg l^{-1} in spring and fall respectively) (Fig. 4; Supplementary Table 1). The lower TChl-a was observed in the 200 m depth stations in both seasons (<0.03 μg l^{-1}). The lack of samples at 200 m depth during spring impaired comparison between seasons.

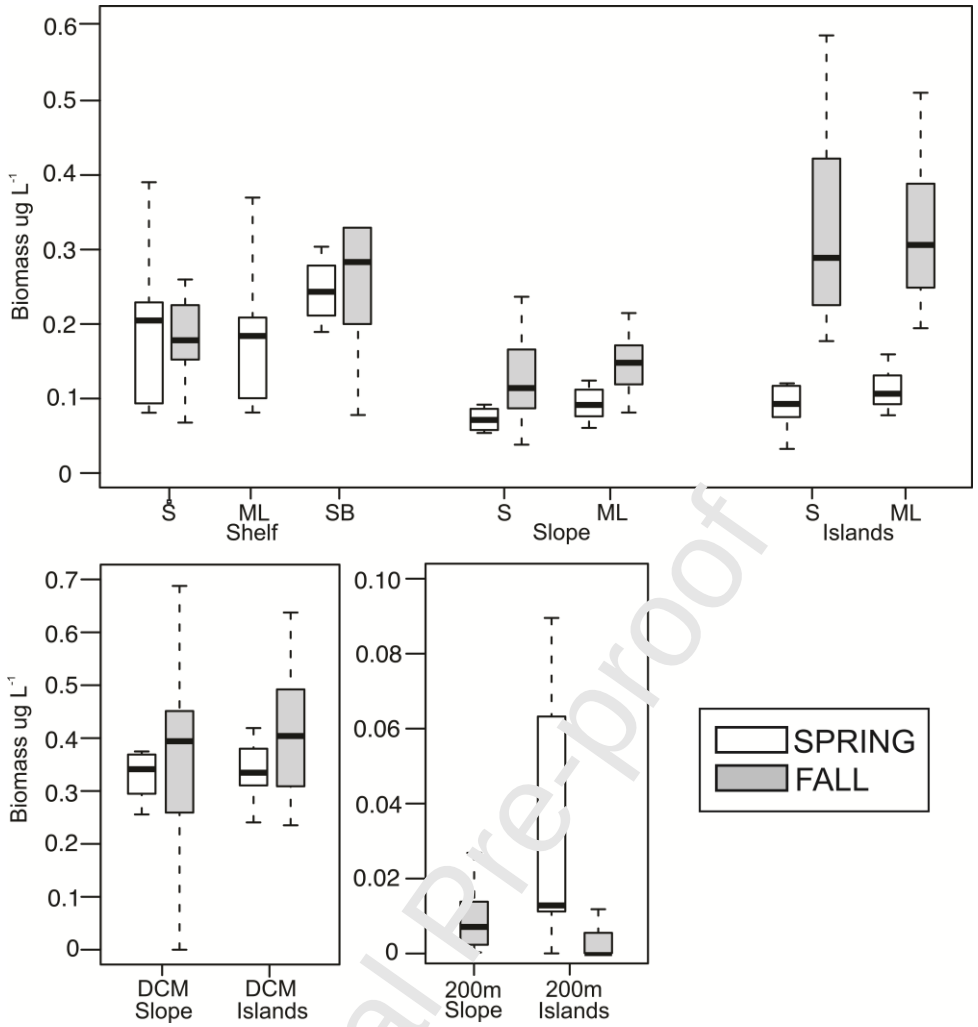

Fig 4. Total phytoplankton biomass (TChl-a concentrations, see Table 1) in the SWTA during spring and fall. S: surface, ML: mixed layer; SB: shallow bottom, DCM: deep chlorophyll maximum. Outliers were removed from the analysis. Notice different y axis scales between plots.

3.3. Pico- and nanophytoplankton vs. microphytoplankton contribution

The Figure 5 represents the pattern in pico- and nanophytoplankton and microphytoplankton contribution for all regions. The pico- and nanophytoplankton (< 20 µm fraction) strongly dominated (>80%) the community regardless the season and depth (Fig. 5). In the Mixed Layer, this fraction accounted for 90% and 80% of the TChl-*a* in spring and fall, respectively (Fig. 5). In fall (no data in spring), at the more productive depths (Shallow Bottom and DCM), the contribution of microphytoplankton

was reduced in comparison with the Mixed Layer, not exceeding 10% of the total biomass. The higher contribution of the microphytoplankton in fall was related to the increase of Dinophyceae (peri) and Bacillariophyceae (fuco) at all depths (Fig. 7).

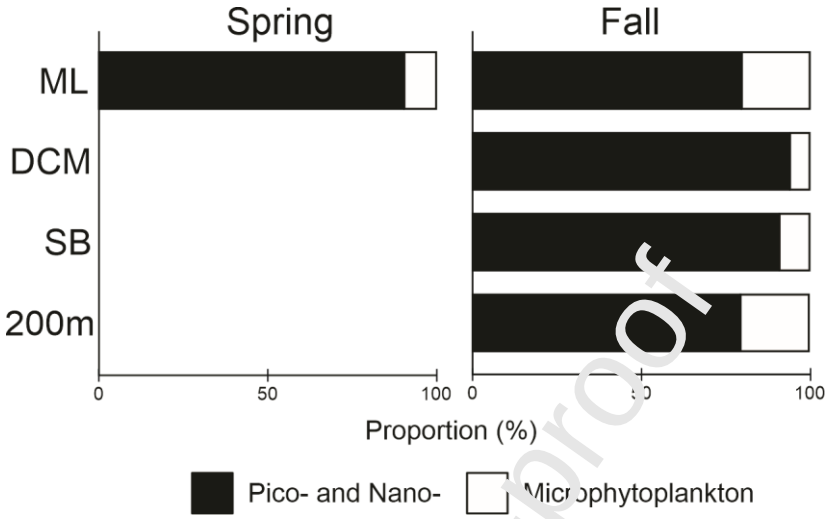

Fig 5. Average relative contribution of pico- and nanophytoplankton, and microphytoplankton to the total biomass (TChl-a concentrations) for all sampling areas. S: surface, ML: mixed layer; SB: shallow bottom, DCM: deep chlorophyll maximum.

3.4. Phytoplankton community structure and distribution

A total of 15 pigments were analyzed: Chl-*a*, Chl-*b*, Chl_{C2}, Chl_{C3}, Peri, 19BF, 19HF, Fuco, Neo, Vio, Dia, Allo, Zea, Div Chl-*a* and Div Chl-*b*. These pigments were used to characterize the dominant taxonomic groups among the phytoplankton community (see Table 1).

Factor	df	MS	Pseudo-F	*p* (MC)
Region	2	2291.1	4.40	0.009
Water Layer	4	33786	65.95	<0.001
Season	1	6888.9	13.24	<0.001

Table 2. Results of PERMANOVA main tests comparing phytoplankton communities among the factors season (spring and fall), region (shelf, continental slope and islands) and water layer (Surface, Mixed Layer, Shallow Bottom, Deep Chlorophyll Maximum and 200 m). MC: Monte Carlo.

The horizontal and vertical patterns of pigments distribution (Fig. 6) showed higher Cyanophyceae (zea) concentration in the surface layer regardless the region and season, although their relative contribution declined in fall, i.e., ~58% and ~40% in spring and fall, respectively (Figs. 6 and 7). An increase of accessory pigments of three phytoplankton groups, Bacillariophyceae (fuco), Dinophyceae (peri) and Chlorophyceae (Chl-*b*, neo, vio) was observed in fall in all regions (Figs. 6 and 7). These differences in community structure were confirmed by the PERMANOVA (Table 2), which pointed out structural community changes among seasons. The Bacillariophyceae pigment increase was more evident over the shelf, going from 20 to 40% of the total accessory pigments in fall (Figs. 6 and 7).

The overall pattern of phytoplankton community was shaped mainly by the pico- and nanophytoplankton (Fig. 5). Microphytoplankton pigments showed a clear dominance of the Bacillariophyceae pigments in the shelf stations, representing up to 80% of the total pigments concentration, whereas offshore a similar vertical and horizontal pattern with the pico- and nanophytoplankton was perceived (see Supplementary Figure 2).

Factor Regions		
Groups	**t**	***p* (MC)**
Shelf, Continental Slope	3.498	<0.001
Shelf, Islands	1.157	0.22
Continental Slope, Islands	2.255	<0.001
Factor Depths		
Groups	**t**	***p* (MC)**
200 m, DCM	5.844	<0.001
200 m, ML	5.984	<0.001
200 m, S	5.632	<0.001
SB, ML	0.974	0.41
SB, S	0.806	0.59
DCM, ML	16.111	<0.001
DCM, S	15.343	<0.001
ML, S	2.693	<0.001

Table 3. Pairwise PERMANOVA results showing comparisons of phytoplankton communities among the factors region (shelf, continental slope and islands) and water layer (S: surface; ML: mixed layer; SB: shallow bottom; DCM; 200 m).

In contrast to surface layers, the pigment concentrations of all groups increased in both seasons in the DCM, especially *Prochlorococcus* (Div Chl-*b*) reaching up to 30% of the community pigment concentrations over the continental slope, which was reflected in the PERMANOVA results, that indicated different communities between the surface layers and DCM (Table 3). The 200 m depth, also showed a contrasting community from the other depths (Table 3), with an increase in the Prymnesiophyceae (19HF) and Dictyochophyceae (19BF) pigments concentration (Fig. 7).

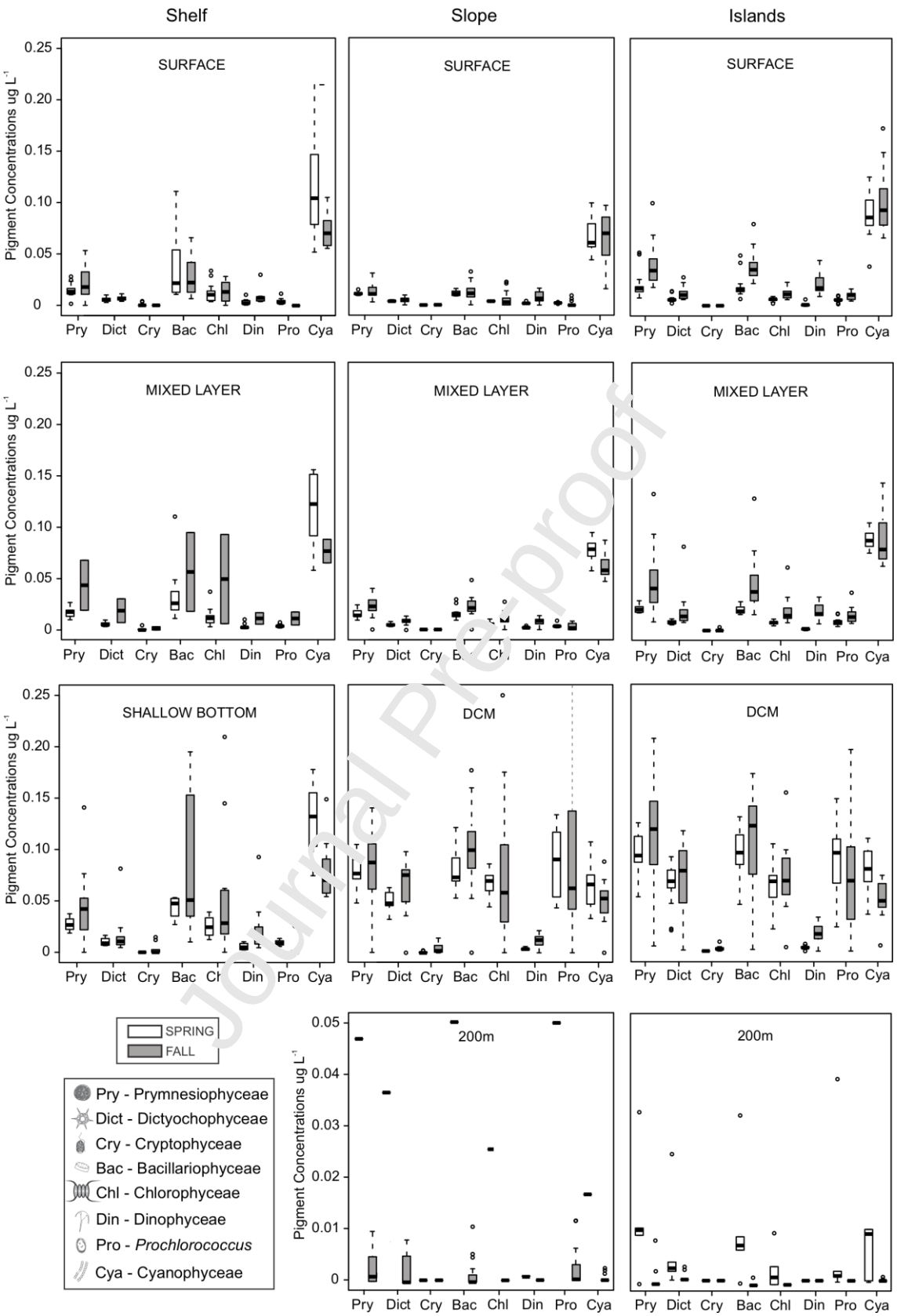

Fig 6. Concentrations of phytoplankton taxa pigment biomarkers (as indicated in Table 1) in the SWTA during spring and fall for all regions and depths. Notice the different scale in the 200 m plots. DCM: deep chlorophyll maximum.

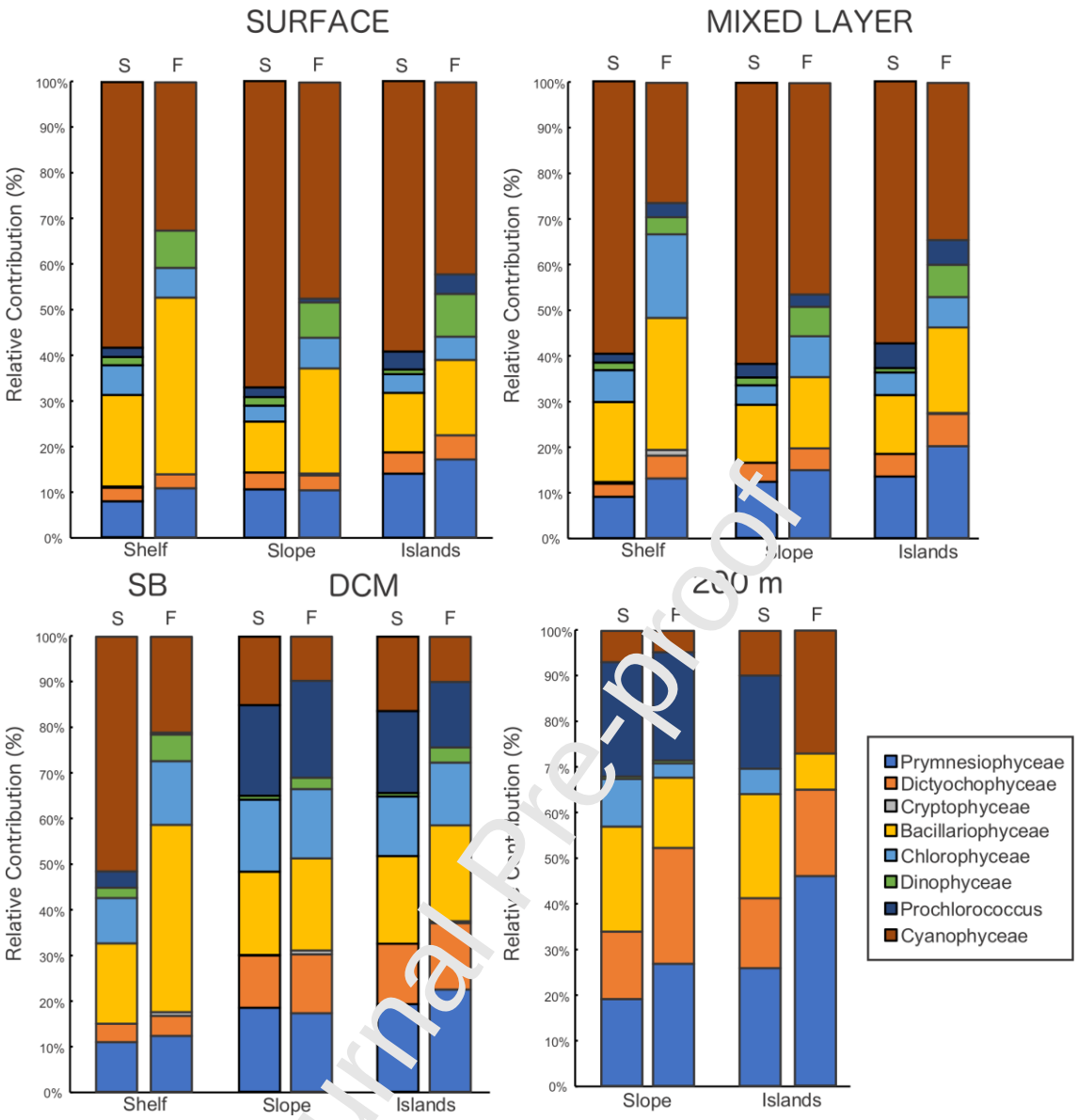

Fig 7. Relative contribution of phytoplankton taxa pigment biomarkers (as indicated in Table 1) to the total pigments concentrations in the SWTA during spring and fall as a proxy of each taxa contribution to total biomass. S: spring; F: fall; SB: shallow bottom; DCM: deep chlorophyll maximum.

3.5. Environmental variability and phytoplankton community

GAMs models assessing the influence of environmental parameters on the total (TChl-a) or individual taxa explained at least 40% of the total variance (Table 4). Depth was the main predictor of the TChl-a in both seasons with the higher biomass in 50 m (spring) and 125 m (fall), which represented the main DCM depth in both seasons. Depth was also the main predictor for Prymnesiophyceae (19HF), Dictyochophyceae

(19BF) and *Prochlorococcus* (Div Chl-*b*), which displayed their higher accessory pigment concentrations near the DCM in both seasons, although the later presented small variability in spring (Fig. 8b). Cyanophyceae (zea) displayed a decrease in concentration with depth (Fig 8b), highlighting their association with the shallow layer. Besides depth, salinity and SiO_4^{-4} were significant predictors for the whole community distribution, with an increase in biomass associated to salinity 37, in spring, and an inverse relation between salinity and TChl-a, in fall. In both seasons, SiO_4^{-4} values above 1 µmol l^{-1} were also associated to a phytoplankton biomass increase (Fig 8a). This pattern was observed for Bacillariophyceae (fuco; both seasons), Cryptophyceae (allo; spring) and Chlorophyceae (Chl-*b*, neo, vio; fall), that showed SiO_4^{-4} as their main predictor (Fig 8b). In spring, NOx was the main predictor for Chlorophyceae (Chl-*b*, neo, vio) distribution, with the higher importance of this phytoplankton group between concentrations of 1 and 2 µmol l^{-1} (Fig. 8b). Considering the spatial variability, only the continental slope was significant and associated to the lower biomass (Fig. 8a).

	Model	Season	R^2	GCV
Pry	*pry* = ***s(Depth)*** + *s(Sal)* + *s(NOx)* + *regions*	Spring	0.93	0.9×10^{-4}
	pry = ***s(Depth)*** + *s(Sal)* + *regions*	Fall	0.69	0.6×10^{-3}
Dict	*dict* = ***s(Depth)*** + *s(NOx)* + *regions*	Spring	0.95	0.4×10^{-4}
	dict = ***s(Depth)*** + *s(Sal)* + *regions*	Fall	0.76	0.3×10^{-3}
Cry	*cry* = *s(Sal)* + ***s(SiO₄)*** + *s*(PO_4^{3-}) + *regions*	Spring	0.40	0.2×10^{-6}
	cry = ***s(Depth)*** + *s(Sal)* + *regions*	Fall	0.60	0.4×10^{-5}
Bac	*bac* = ***s(Depth)*** + *s(Sal)* + ***s(SiO₄)*** + *s*(PO_4^{3-}) + *regions*	Spring	0.94	0.1×10^{-3}
	bac = ***s(Depth)*** + *s(Sal)* + ***s(SiO₄)*** + *s*(PO_4^{3-}) + *regions*	Fall	0.84	0.2×10^{-3}
Chl	*chl* = ***s(Depth)*** + *s(Sal)* + ***s(NOx)***+ *s(SiO)* + *s*(PO_4^{3-}) + *regions*	Spring	0.95	0.3×10^{-4}
	chl = ***s(Depth)*** + *s(Sal)* + ***s(SiO₄)*** + *regions*	Fall	0.73	0.6×10^{-3}
Din	*din* = ***s(Sal)*** + *regions*	Spring	0.51	0.3×10^{-5}
	din = ***s(Depth)*** + *s(Sal)* + *s(BLT)* + *regions*	Fall	0.67	0.3×10^{-4}
Cya	*cya* = ***s(Depth)*** + *s(Sal)* + *s(MLD)* + *regions*	Spring	0.70	0.1×10^{-2}
	cya = ***s(Depth)*** + *s(Sal)* + *s(MLD)* + *regions*	Fall	0.82	0.03×10^{-2}
Pro	*pro* = ***s(Depth)*** + *s(NOx)* + *s*(PO_4^{3-}) + *regions*	Spring	0.92	0.6×10^{-4}
	pro = ***s(Depth)***	Fall	0.73	0.3×10^{-3}
TChl-a	*tchl-a* = ***s(Depth)*** + *s(Sal)* + *s*(SiO_4) + *regions*	Spring	0.89	0.2×10^{-2}
	tchl-a = ***s(Depth)*** + *s(Sal)* + *s*(SiO_4) + *regions*	Fall	0.71	0.2×10^{-2}

Table 4. Statistical summary of generalized additive models between the biomass of the different taxa and the environmental parameters. R^2 is the adjusted proportion of total variability explained by the model. GCV: generalized cross validation score; NOx: NO_3- + NO_2; Depth; Sal: salinity; TChl-a: total biomass; MLD: mixed layer depth; BLT: barrier layer thickness Pry: Prymnesiophyceae; Dict: Dictyochophyceae; Cry: Cryptophyceae; Bac: Bacillariophyceae; Chl: Chlorophyceae; Din: Dinophyceae; Pro: *Prochlorococcus*; Cya: Cyanophyceae; n = 101 (spring) and 160 (fall). In bold are the main predictors of the taxa in each model.

3.5. New Biomass vs. Recycled Biomass

The phytoplankton trophic status was studied based on the *Fp* index representing the biomass ratio of the phytoplankton involved in the new production (Bacillariophyceae and Dinophyceae) over the total phytoplankton (Table 5). Overall, the average new production associated to Bacillariophyceae (fuco) and Dinophyceae (peri) was low, not surpassing 0.21 (Table 5). In both seasons, the new biomass was higher over the shelf (average *Fp* in the Shallow Bottom ranging from 0.10 to 0.21 in spring and fall, respectively). The continental slope and islands stations showed similar *Fp* in the Mixed Layer and DCM, with an average *Fp* of 0.09 (Table 5). An increase in the *Fp* value of all regions in fall was noticed, altnough it was only significant in the islands surface layer (Surface and Mixed Layer) (t-test, $p < 0.001$).

		Shelf	Slope	Islands			Shelf	Slope	Islands
Spring	S	0.13	0.06	0.04	Fall	S	0.18	0.06	**0.09**
	ML	0.11	0.07	0.04		ML		0.09	**0.09**
	SB	0.10				SB	0.21		
	DCM		0.05	0.06		DCM		0.07	0.06
	200m			0.04		200m			
Average		0.11	0.06	0.045			0.19	0.07	0.08

Table 5. *Fp* index value for all regions and depths in both seasons in the SWTA. In bold values that were significantly higher in that season. S: surface; ML: mixed layer; SB: shallow bottom; DCM: deep chlorophyll maximum.

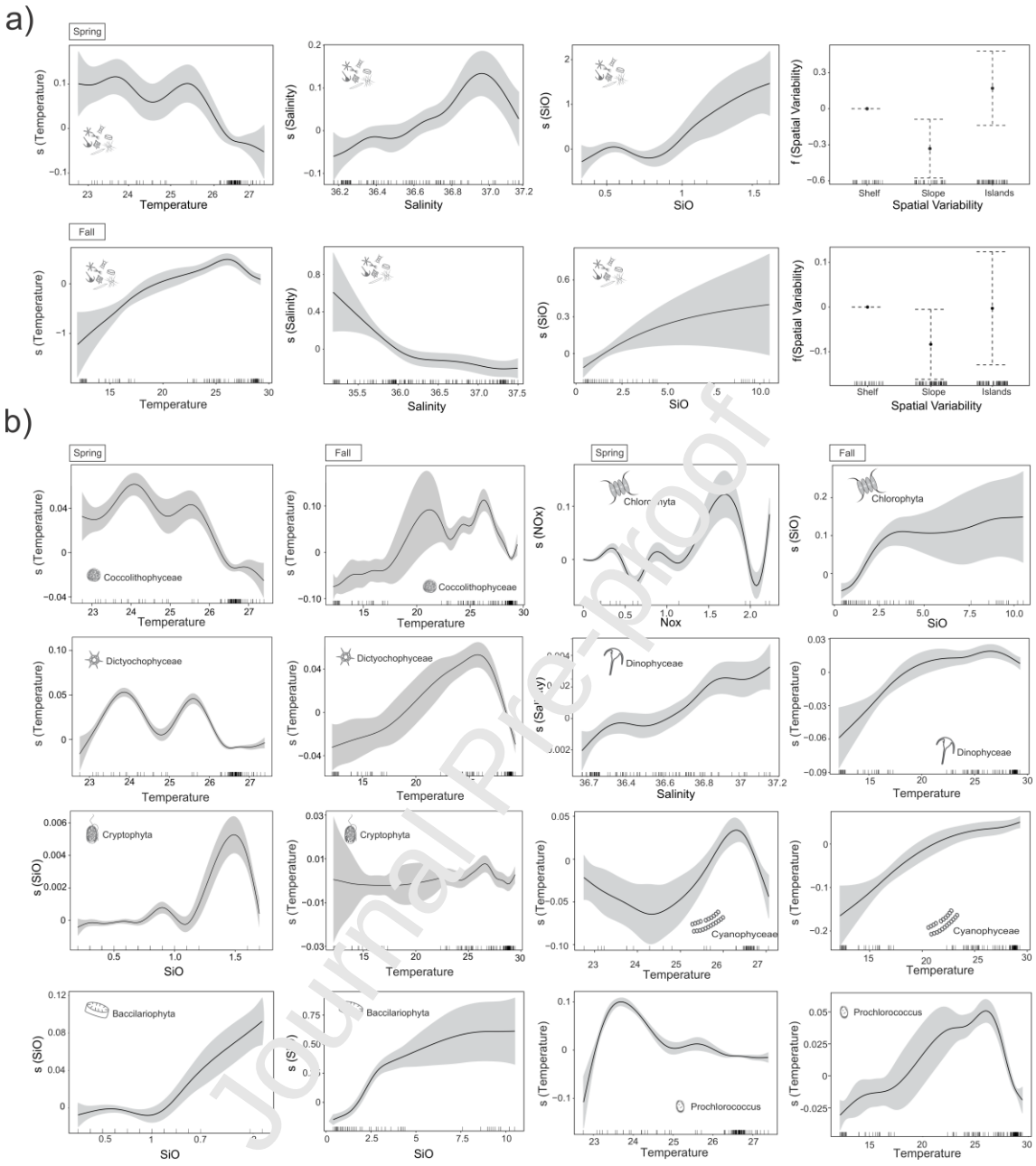

Fig 8. Generalized Additive Models (GAMs) results describing the main factors that influenced the phytoplankton, for the entire community (a) and for the identified groups in both seasons (b). Solid lines represent smoothed mean relationships from GAM's and shaded areas are 95% confidence intervals.

4. Discussion

Our results pointed out a mosaic-like phytoplankton distribution mainly shaped by the thermohaline structure governing the SWTA, which during fall promoted a shallower depth of mixed layer and nutricline, thereby favoring a higher phytoplankton biomass. Along with such environmental configuration, the phytoplankton biomass displayed clear seasonal differences, although the contribution of pico- and nanophytoplankton to total phytoplankton biomass was similar regardless the season, suggesting an uncoupled dynamics between phytoplankton size structure and biomass production.

4.1. *Influence of physical oceanographic structures on nutrients and biomass distribution*

The nutrients concentration showed a general increase with depth, excepting NO_2^-, which formed a primary nitrite maximum in the continental slope and oceanic islands DCM. Such feature has been previously reported from field records in oligotrophic stratified waters (Lomas and Lipschultz, 2006; Mackey et al., 2011), including in the SWTA (Paulo, 2016; Souza et al., 2013). The primary nitrite maximum may be related with both the excretion of NO_2^- by phytoplankton, i.e., due to incomplete nitrate reduction, and with the nitrification of bacteria (Al-Qutob et al. 2002; Meeder et al. 2012), although this should be confirmed with further field experiments. In addition, it is worth noticing the observed dominance of *Prochlorococcus* in the primary nitrite maximum. Indeed, this Genus has been formerly linked to the accumulation of nitrite in the water column due to the incomplete nitrate reduction of low light adapted ecotypes (Berube et al., 2016).

In fall, the depth of thermocline favored a shallower nutricline, thus increasing nutrients availability in upper layers. However, in spring, some stations near Fernando de Noronha Archipelago and Rocas Atoll displayed an increase of nutrients at DCM

similar to the concentration recorded at 200 m depth. In addition, the interaction of oceanic islands and seamounts with the dynamics of water masses promotes an Island Mass Effect that foster productivity in the open ocean (Doty and Oguri 1956; Boden 1988; Hasegawa et al. 2008). In the SWTA, such island mass effect has been observed in both nutrients concentration and plankton productivity (Chaves et al., 2006; Macedo et al., 1988; Melo et al., 2012; Souza et al., 2013). This phenomenon exhibits a marked seasonality, mainly occurring in the western region of the oceanic islands between March and July, concurrently with the enhancement of the South Equatorial Current (Tchamabi et al., 2017; Travassos et al., 1997). Also, during spring strong vertical shear, topographically induced, was observed between the surface South Equatorial Current and the subsurface South Equatorial Under Current, forming mesoscale meanders and a subsurface eddy-like structure, which likely contributed to the observed nutrients increase. However, such feature was not reflected in phytoplankton biomass, probably due to a lag in phytoplankton response. An alternative explanation may be linked to a phosphate limitation during the upwelling event, as suggested by the observed Redfield Ratio of 24:1.

In all other stations, the observed nutrients concentration is in line with previous reports in the area that showed similar seasonal patterns (Hazin, 2009; Souza et al., 2013). Likewise, surface nitrogen concentrations, under 1 μmol l^{-1}, were similar to values reported for other stratified oligotrophic waters (Islabão et al., 2017; Mena et al., 2019). However, compared with other regions it is worth noticing that the N:P ratio of about 3:1, was markedly lower than the ratio observed in the Tropical Eastern Pacific (7-10:1) and in the Mediterranean Sea (5:1) (Mena et al., 2019; Yasunaka et al., 2019). Overall, our records pointed out a nitrogen limitation with a N:P local ratio lower than the Redfield Ratio (16:1).

Nutrients availability in the SWTA are closely connected to seasonal patterns of dominant physical structures. For instance, the continental slope DCM showed lower nutrients concentration than the oceanic islands, regardless the season. The continental slope further showed the thickest thermocline and larger barrier layer, although the latter was not evenly distributed throughout the region (Assunção et al., 2020). Such physical barrier shape productivity of shallow waters preventing vertical transport from deep cold nutrient-rich waters to surface. (Cabrera et al., 2011; Qu and Meyers, 2005). Nevertheless, over the continental slope, surface layers showed higher NO_3^- concentrations than around the islands, likely due to the activity of diazotrophic Cyanophyceae, which is the main group responsible for nitrogen fixation in tropical oceans (LaRoche and Breitbarth, 2005) and was more abundant in this region.

Phytoplankton biomass was generally low, with maxima lower than 1.8 µg l^{-1}, although a seasonal increase was observed in surface layers of islands stations. Souza et al. (2013) also noticed an increase in chl-a concentration from late summer to fall around the oceanic islands, although with higher biomass (~ 0.47 µg l^{-1} in the mixed layer). In addition, these authors observed a higher nitrogen availability than the one measured in this study, which also exhibit a similar low N:P ratio (5:1), thus suggesting a nitrogen limitation to primary production, as observed here. It is worth noticing that in fall higher nitrate concentrations in surface waters of the continental slope were uncoupled from phytoplankton biomass, which was almost three times lower than shelf and oceanic islands stations, possible due to zooplankton grazing, as suggested by maximum zooplankton abundance recorded in the continental slope (Figueiredo et al., 2020).

In this region, the variability of phytoplankton biomass has been previously ascribed to the seasonality of riverine nutrient inputs and upwelling events promoted by

the Island Mass Effect and Taylor column effect (Ekau and Knoppers, 1999; Otsuka et al., 2018; Souza et al., 2013). Furthermore, TChl-a concentration in oligotrophic oceans is characterized by seasonal changes that follow the intensity of the mixed layer, thus increasing when the mixed layer is deeper and reaching the nutricline (Mignot et al., 2014; Signorini et al., 2015). In our study, we found a different pattern with a biomass increase in the shallower mixed layer and nutricline that was linked to the shallower thermocline. Our results suggest a pivotal role played by the vertical thermohaline structure in the seasonal variability of phytoplankton.

4.2.Phytoplankton community dynamics associated with environmental variability

Phytoplankton dynamics was shaped by water column vertical stratification, displaying marked changes in the distribution of phytoplankton, particularly between surface (Surface and Mixed Layer) and deep waters (DCM and 200 m depth), with a more diverse community in the latter. In surface layers, Cyanophyceae were dominant. This group is known to flourish in oligotrophic communities worldwide (Karlusich et al., 2020; Queiroz et al., 2015), contributing to ~25% of the ocean net primary productivity (Lange et al., 2018) and having an essential role in the oceanic nitrogen cycle, due to their ability to use atmospheric nitrogen. Indeed, this feature allows the group dominating low nitrogen-to-phosphorus environments, such as the SWTA (Vrede et al., 2009). With depth increase and the overall decrease of other Cyanophyceae, *Prochlorococcus* flourished. *Prochlorococcus* inhabits a wide range of depths from the surface waters to the base of the euphotic zone, due to their variable genetic ecotypes adapted to growth at high or low-light intensities (Moore et al., 1998). In communities dominated by the low-light adapted ecotypes, higher biomasses near the DCM are likely to be reached, as observed in oligotrophic oceans (Berube et al., 2016; Hawco et al., 2021). These ecotypes display a prochlorophyte chlorophyll-binding protein, which

together with divinyl chlorophyll-*b* allows low-light adapted ecotypes a higher absorption of the blue light presented in deeper layers (Islabão et al., 2017). Although we did not distinguish ecotypes, *Prochlorococcus* biomass increased near the DCM, and the known relation with the nitrite primary maximum formation may indicate the dominance of low-light adapted *Prochlorococcus* in the SWTA phytoplankton community.

The observed higher biomass of Chlorophyceae over the shelf, near the surface, and the biomass increase during fall may be indicative of riverine discharges, as this group is mostly composed by freshwater species (Mishra et al., 2009). Similarly, Bacillariophyceae are also abundant near the shelf, favored by the higher silicate concentrations, this trend was evident in the microphytoplankton pigments, which, although displayed low biomass, was dominated by the Bacillariophyceae. In oligotrophic regions, diatoms are commonly more abundant in the inner shelf than in oceanic regions, due to higher silicates availability and a weaker thermocline stratification (Falkowski and Oliver, 2007; Mishra et al., 2020). However, Dinophyceae relative biomass was low at both seasons, with a slight increase in fall. This is likely underestimated by our pigment analysis, as this group is composed by a variety of trophic strategies, i.e., autotrophic, mixotrophic and heterotrophic, that may represent ca. 50% of the dinoflagellate's community (Hansen, 2011; Jeong et al., 2010; Sherr and Sherr, 2007). In addition, other dinoflagellates can be characterized by different pigments, such as fucoxanthin or chlorophyll-*b*, which suggest a possible underestimating of this groups (Zapata et al., 2012).

Prymnesiophyceae and Dictyochophyceae were more frequent in the light-limited and nutrient rich deep layers. Prymnesiophyceae show low light and nitrate saturation for growth (Araujo et al., 2017), thus this group can thrive in regions

constraining growth of other groups, such as Bacillariophyceae and Chlorophyceae, as seem to be the case here (Araujo et al., 2017; Gregg and Casey, 2007). On the other hand, Dictyochophyceae are widespread in the marine environments, especially in the subtropical and temperate regions (Andersen, 2004) composing mostly the microphytoplankton, ranging usually between 20 and 100 µm (Lemonnier et al., 2016). In the HPLC analysis, this group is represented by the larger silicoflagellate *Dictyocha* sp., and small picoflagellates and picoeukaryotes. Therefore, due to the main representation of the pico- and nanophytoplankton in the SWTA phytoplankton community, Dictyochophyceae is likely composed by small cells, although more specific analyses are needed to unveil the composition of this group.

4.3. Size structure and trophic status

Cell size is an ecological trait that affects all aspects of phytoplankton ecology, such as diversity, production, competition, and biomass transference to the higher trophic levels (Barton et al., 2013; Marañón, 2015). We observed a dominance of pico- and nanophytoplankton in both seasons, in agreement with reported observations in many oligotrophic regions (Dai et al., 2020; Mena et al., 2019; Pérez et al., 2005). These small sized communities are usually associated with recycling trophic webs. The *Fp* index is derived from the assumption that global new production is mainly related to diatoms growth, while dinoflagellates growth is less relevent (Claustre, 1994). This qualitative tool allows comparing trophic status of some oceanographic regimes and inferring about the size dynamics of a community. In the southernmost area of the tropical Atlantic, a preeminence of recycling productivity was previously reported, with the new production representing between 16 and 30% of the total phytoplankton production (Metzler et al., 1997). Our results pointed out a predominance of recycled production, with a conspicuous coast-offshore gradient evidenced by the observed higher *Fp* in the shelf,

which was double than in other regions, likely due to the influence of the riverine runoffs on the coast productivity (Ekau and Knoppers, 1999; Otsuka et al., 2018). In addition, a significant seasonal increase in the new production was observed in oceanic islands, although, the values remained low and did not surpass 0.09, suggesting a dominance of small cells also in punctual productivity peaks.

The overall increase in nutrients concentration usually results in an enhancement of large phytoplankton cells and a change in the trophic balance to a more classic food web instead of a microbial one (Chisholm, 1992; Falkowski and Oliver, 2007; Landry, 2002; Vargas et al., 2007). However, in oligotrophic regions of the Atlantic Ocean there is an uncoupled relationship between productivity and phytoplankton size. Indeed, even during enhanced production and biomass, the dominance of pico- and nanophytoplankton remains (Marañón et al., 2003, 2000). Our observations support the hypothesis of the smaller cells (<20 µm) dominating the community, with a change in the trophic status only in a few shelf stations that showed high *Fp* (<0.5). The pico- and nanophytoplankton predominance probably is linked to the low N:P (<5), which appears insufficient to trigger a pronounced growth of larger cells. Nitrogen has been previously observed as a limiting nutrient for the phytoplankton growth in the SWTA (Hazin, 2009), with a N:P ratio in the euphotic zone lower than 5:1 throughout the year.

Large phytoplankton cells (i.e., diatoms and dinoflagellates) play an important role in carbon sequestration, due to their higher sinking rate in contrast to smaller phytoplankton cells (Guidi et al., 2016). In oligotrophic oceans however, their role in the carbon pump is replaced by small phytoplankton cells (Guidi et al., 2016; Weinbauer, 2004), which may form colloids and aggregates in the water column enhancing their rates of sedimentation. In a global change scenario, the expansion of

oligotrophic oceans and higher stratified waters are expected, with predominance of microbial food webs. Understanding the role of such small phytoplankton groups in the carbon pump is therefore crucial to assess not only changes in biogeochemical cycling, but also changes in food quality for pelagic food webs.

5. Conclusions

In the SWTA phytoplankton community, an uncoupling between the biomass increase and size was observed, with the phytoplankton being dominated by the small celled community and a recycled production (*Fp*) during the entire study time. Here we hypothesize that this may be caused by a nitrogen limitation that constrain population growth of the large phytoplankton taxa. In the SWTA this was the first study to analyze the contribution of the phytoplankton different size classes offshore. The domination of the pico- and nanophytoplankton presented here, highlights their importance to the global oligotrophic oceans. In the scenario of global ocean changes, in which water column stratification is expected to intensify, the abundance of this small phytoplankton and the recycling production will probably rise. Thus, the understanding of their distribution and role in the biogeochemical cycles is of pivotal importance to forecast the health of the pelagic food webs in the near future.

Acknowledgements

We wish to express our thanks to the Coordenação de Aperfeiçoamento de Pessoal de Nível Superior – Brasil (CAPES) for the concession of the first author's scholarship, and the IMAGO lab who realized the HPLC and nutrients analysis. We acknowledge the French oceanographic fleet for funding the survey ABRACOS and the officers, crew and scientific team of the R/V Antea for their contribution to the success of the operations. This work is a contribution to the LMI TAPIOCA (www.tapioca.ird.fr), CAPES/COFECUB program (88881.142689/2017-01), the

European Union's Horizon 2020 projects PADDLE (grant agreement No. 73427) and TRIATLAS (grant agreement No. 817578).

References

Al-Qutob, M., Häse, C., Tilzer, M.M., Lazar, B., 2002. Phytoplankton drives nitrite dynamics in the Gulf of Aqaba, Red Sea. Mar. Ecol. Prog. Ser. 239, 233–239. https://doi.org/10/bz4r7c

Andersen, R.A., 2004. Biology and systematics of heterokont and haptophyte algae. Am. J. Bot. 91, 1508–1522. https://doi.org/10.3732/ajb.91.10.1508

Araujo, M., Limongi, C., Servain, J., Silva, M., Leite, F.S., Veleda, D., Lentini, C.A.D., 2011. Salinity-induced mixed and barrier layers in the southwestern tropical Atlantic Ocean off the northeast of Brazil. Ocean Sci. 7, 63–73. https://doi.org/10/b3fhtj

Araujo, M.L.V., Mendes, C.R.B., Tavano, V.M., Garcia, C.A.E., Baringer, M.O., 2017. Contrasting patterns of phytoplankton pigments and chemotaxonomic groups along 30°S in the subtropical South Atlantic Ocean. Deep Sea Res. Part Oceanogr. Res. Pap. 120, 112–121. https://doi.org/10/gf7kmx

Assunção, R.V., Silva, A.C., Roy, A., Bourlès, B., Silva, C.H.S., Ternon, J.-F., Araujo, M., Bertrand, A., 2020. 3D characterisation of the thermohaline structure in the southwestern tropical Atlantic derived from functional data analysis of in situ profiles. Prog. Oceanogr. 187, 102399. https://doi.org/10.1016/j.pocean.2020.102399

Barton, A.D., Pershing, A.J., Litchman, E., Record, N.R., Edwards, K.F., Finkel, Z.V., Kiorboe, T., Ward, B.A., 2013. The biogeography of marine plankton traits. Ecol Lett 16, 522–534. https://doi.org/10/f4sqgs

Bell, T., Kalff, J., 2001. The contribution of picophytoplankton in marine and freshwater systems of different trophic status and depth. Limnol. Oceanogr. 46, 1243–1248. https://doi.org/10.4319/lo.2001.46.5.1243

Berube, P.M., Coe, A., Roggensack, S.E., Chisholm, S.W., 2016. Temporal dynamics of Prochlorococcus cells with the potential for nitrate assimilation in the subtropical Atlantic and Pacific oceans. Limnol. Oceanogr. 61, 482–495.

Bertrand, A., 2017. ABRACOS 2 cruise, Antea R/V. https://doi.org/10.17600/17004100

Bertrand, A., 2015. ABRACOS cruise, Antea R/V. https://doi.org/10.17600/15005600

Boden, B.P., 1988. Observations of the island mass effect in the Prince Edward archipelago. Polar Biol. 9, 61–68. https://doi.org/10.1007/BF00441765

Burson, A., Stomp, M., Greenwell, E., Grosse, J., Huisman, J., 2018. Competition for nutrients and light: testing advances in resource competition with a natural phytoplankton community. Ecology 99, 1108–1118. https://doi.org/10.1002/ecy.2187

Cabrera, O., Villanoy, C., David, L., Gordon, A., 2011. Barrier Layer Control of Entrainment and Upwelling in the Bohol Sea, Philippines. Oceanography 24, 130–141. https://doi.org/10/cvppt7

Castello, J.P., 2010. O futuro da pesca da aquicultura marinha no Brasil: a pesca costeira. Ciênc. E Cult. 62, 32–35.

Chaves, T., Mafalda, J., Santos, C., Souza, C., Moura, G., Sampaio, J., Melo, G., Passavante, J., Feitosa, F., 2006. Planktonic biomass and hydrography in the Exclusive Economic Zone of Brazilian Northeast. Trop. Oceanogr. Online 34, 12–30.

Chisholm, S.W., 1992. Phytoplankton Size, in: Falkowski, P.G., Woodhead, A.D., Vivirito, K. (Eds.), Primary Productivity and Biogeochemical Cycles in the Sea, Environmental Science Research. Springer US, Boston, MA, pp. 213–237. https://doi.org/10.1007/978-1-4899-0762-2_12

Clarke, K.R., Gorley, R.N., 2006. PRIMER V6: user manual-tutorial. Plymouth Marine Laboratory.

Claustre, H., 1994. The trophic status of various oceanic provinces as revealed by phytoplankton pigment signatures. Limnol. Oceanogr. 39, 1206–1210. https://doi.org/10/fj9bb6

da Silveira, I.C.A., Schmidt, A.C.K., Campos, E.J.D., de Godoi, S.S., Ikeda, Y., 2000. A corrente do Brasil ao largo da costa leste brasileira. Rev Bras Ocean 48, 171–183. https://doi.org/10/gf4mq3

Dai, S., Zhao, Y., Li, X., Wang, Z., Zhu, M., Liang, J., Liu, H., Tian, Z., Sun, X., 2020. The seamount effect on phytoplankton in the tropical western Pacific. Mar. Environ. Res. 105094. https://doi.org/10/gg72jv

Dandonneau, Y., Deschamps, P.Y., Nicolas, J.M., Loisel, H., Blanchot, J., Montel, Y., Thieuleux, F., Bécu, G., 2004. Seasonal and interannual variability of ocean color and composition of phytoplankton communities in the North Atlantic, equatorial Pacific and South Pacific. Deep Sea Res. Part II Top. Stud. Oceanogr., Views of Ocean Processes from the Sea-viewing Wide Field-of-view Sensor (SeaWiFS) Mission: Volume 1 51, 303–318. https://doi.org/10.1016/j.dsr2.2003.07.013

Dossa, A.N., Silva, A.C., Chaigneau, A., Eldin, G., Araujo, M., Bertrand, A., 2021. Near-surface western boundary circulation off Northeast Brazil. Prog. Oceanogr. 190, 102475. https://doi.org/10.1016/j.pocean.2020.102475

Doty, M.S., Oguri, M., 1956. The island mass effect. ICES J. Mar. Sci. 22, 33–37. https://doi.org/10.1093/icesjms/22.1.33

Egge, J.K., 1998. Are diatoms poor competitors at low phosphate concentrations? J. Mar. Syst. 16, 191–198. https://doi.org/10/d3747t

Ekau, W., Knoppers, B., 1999. An introduction to the pelagic system of the North-East and East Brazilian shelf. Arch. Fish. Mar. Res. 47, 113–132.

Falkowski, P.G., Oliver, M.J., 2007. Mix and match: how climate selects phytoplankton. Nat. Rev. Microbiol. 5, 813–819. https://doi.org/10/chrd2m

Figueiredo, G.G.A.A. de, Schwamborn, R., Bertrand, A., Munaron, J.M., Le Loc'h, F., 2020. Body size and stable isotope composition of zooplankton in the western tropical Atlantic. J. Mar. Syst. 212, 103449. https://doi.org/10.1016/j.jmarsys.2020.103449

Finkel, Z.V., Beardall, J., Flynn, K.J., Quigg, A., Rees, T.A.V., Raven, J.A., 2010. Phytoplankton in a changing world: cell size and elemental stoichiometry. J. Plankton Res. 32, 119–137. https://doi.org/10/bb25d7

Flombaum, P., Gallegos, J.L., Gordillo, R.A., Rincón, J., Zabala, L.L., Jiao, N., Karl, D.M., Li, W.K.W., Lomas, M.W., Veneziano, D., Vera, C.S., Vrugt, J.A., Martiny, A.C., 2013. Present and future global distributions of the marine Cyanobacteria Prochlorococcus and Synechococcus. Proc. Natl. Acad. Sci. 110, 9824–9829. https://doi.org/10/f436jc

Grasshoff, Klaus, M. Ehrhardt, e K. Kremling. *Methods of seawater analysis*. Weinheim: Verlag Chemie, 1983.

Gregg, W.W., Casey, N.W., 2007. Modeling coccolithophores in the global oceans. Deep Sea Res. Part II Top. Stud. Oceanogr., The Role of Marine Organic Carbon and Calcite Fluxes in Driving Global Climate Change, Past and Future 54, 447–477. https://doi.org/10/fxbzsg

Guidi, L., Chaffron, S., Bittner, L., Eveillard, D., Larhlimi, A., Roux, S., Darzi, Y., Audic, S., Berline, L., Brum, J., Coelho, L.P., Espinoza, J.C.I., Malviya, S., Sunagawa, S., Dimier, C., Kandels-Lewis, S., Picheral, M., Poulain, J., Searson, S., Tara Oceans, coordinators, Stemmann, L., Not, F., Hingamp, P., Speich, S., Follows, M., Karp-Boss, L., Boss, E., Ogata, H., Pesant, S., Weissenbach, J., Wincker, P., Acinas, S.G., Bork, P., de Vargas, C., Iudicone, D., Sullivan, M.B., Raes, J., Karsenti, E., Bowler, C., Gorsky, G., 2016. Plankton networks driving carbon export in the oligotrophic ocean. Nature 532, 465–470. https://doi.org/10/f8ktsd

Hansen, P.J., 2011. The Role of Photosynthesis and Food Uptake for the Growth of Marine Mixotrophic Dinoflagellates1. J. Eukaryot. Microbiol. 58, 203–214. https://doi.org/10/d9czss

Hasegawa, D., Yamazaki, H., Ishimaru, T., Nagashima, H., Koike, Y., 2008. Apparent phytoplankton bloom due to island mass effect. J. Mar. Syst., Physical-Biological Interactions in the Upper Ocean 69, 238–246. https://doi.org/10.1016/j.jmarsys.2006.04.019

Hastie, T., Tibshirani, R., 1987. Generalized Additive Models: Some Applications. Journal of the American Statistical Association 82, 371–386. https://doi.org/10.1080/01621459.1987.10478440

Hawco, N.J., Fu, F., Yang, N., Hutchins, D.A., John, S.G., 2021. Independent iron and light limitation in a low-light-adapted Prochlorococcus from the deep chlorophyll maximum. ISME J. 15, 359–362. https://doi.org/10.1038/s41396-020-00776-y

Hazin, F.H.V., 2009. Coleção Programa REVIZEE Score Nordeste. Martins & Cordeiro.

Hooker, S.B., Rees, N.W., Aiken, J., 2000. An objective methodology for identifying oceanic provinces. Prog. Oceanogr. 45, 313–338. https://doi.org/10/fns4hr

Islabão, C.A., Mendes, C.R.B., Detoni, A.M.S., Odebrecht, C., 2017. Phytoplankton community structure in relation to hydrographic features along a coast-to-offshore transect on the SW Atlantic Continental Shelf. Cont. Shelf Res. 151, 30–39. https://doi.org/10/ggs2dn

Jardine, J., Palmer, M., Mahaffey, C., Holt, J., Mellor, A., Wakelin, S., 2017. Rainfall as a trigger for stratification and winter phytoplankton growth in temperate shelf seas 19, 6828.

Jeong, H.J., Yoo, Y.D., Kim, J.S., Seong, K.A., Kang, N.S., Kim, T.H., 2010. Growth, feeding and ecological roles of the mixotrophic and heterotrophic dinoflagellates in marine planktonic food webs. Ocean Sci. J. 45, 65–91. https://doi.org/10/c7sjzw

Karlusich, J.J.P., Ibarbalz, F.M., Bowler, C., 2020. Phytoplankton in the *Tara* Ocean. Annu. Rev. Mar. Sci. 12, 233–265. https://doi.org/10/ggh684

Kikuchi, R.K.P., 2002. Atol das Rocas, Litoral do Nordeste do Brasil-Único atol do Atlântico Sul Equatorial Ocidental. Sítios Geológicos E Paleontológicos Bras. Bras. DNPMCPRM SIGEP 390p.

Knoppers, B., Ekau, W., Figueiredo, A.G., 1999. The coast and shelf of east and northeast Brazil and material transport. Geo-Mar. Lett. 19, 171–178. https://doi.org/10/cxdvxw

Landry, M.R., 2002. Integrating classical and microbial food web concepts: evolving views from the open-ocean tropical Pacific. Hydrobiologia 480, 29–39. https://doi.org/10/cv8mnr

Lange, P.K., Brewin, R.J.W., Dall'Olmo, G., Tarran, G.A., Sathyendranath, S., Zubkov, M., Bouman, H.A., 2018. Scratching Beneath the Surface: A Model to Predict the Vertical Distribution of Prochlorococcus Using Remote Sensing. Remote Sens. 10, 847. https://doi.org/10/gdv5dk

LaRoche, J., Breitbarth, E., 2005. Importance of the diazotrophs as a source of new nitrogen in the ocean. Journal of Sea Research, Iron Resources and Oceanic Nutrients - Advancement of Global Environmental Simulations 53, 67–91. https://doi.org/10.1016/j.seares.2004.05.005

Lemonnier, H., Lantoine, F., Courties, C., Guillebault, D., Nézan, E., Chomérat, N., Escoubeyrou, K., Galinié, C., Blockmans, B., Laugier, T., 2016. Dynamics of phytoplankton communities in eutrophying tropical shrimp ponds affected by vibriosis. Mar. Pollut. Bull. 110, 449–459. https://doi.org/10.1016/j.marpolbul.2016.06.015

Lewington-Pearce, L., Narwani, A., Thomas, M.K., Kremer, C.T., Vogler, H., Kratina, P., 2019. Temperature-dependence of minimum resource requirements alters competitive hierarchies in phytoplankton. Oikos 128, 1194–1205. https://doi.org/10.1111/oik.06060

Litchman, E., de Tezanos Pinto, P., Edwards, K.F., Klausmeier, C.A., Kremer, C.T., Thomas, M.K., 2015. Global biogeochemical impacts of phytoplankton: a trait-based perspective. J. Ecol. 103, 1384–1396. https://doi.org/10/f7v9v2

Litchman, E., Klausmeier, C.A., 2008. Trait-Based Community Ecology of Phytoplankton. Annu. Rev. Ecol. Evol. Syst. 39, 615–639. https://doi.org/10/fnnm3w

Lomas, M.W., Lipschultz, F., 2006. Forming the primary nitrite maximum: Nitrifiers or phytoplankton? Limnol. Oceanogr. 51, 2453–2467. https://doi.org/10/dd87bh

Mabesoone, J.M., Coutinho, P.N., 1970. Litoral and shalow marine geology of Northeastern Brasil. Trop. Oceanogr. 12, 1–214. https://doi.org/10/ggnmd3

Macedo, S., Montes, M., Lins, I., Costa, K., 1988. Revizee. Programa de Avaliação do Potencial Sustentável dos Recursos Vivos da Zona Econômica Exclusiva, SCORE/NE.

Mackey, K.R.M., Bristow, L., Parks, D.R., Altabet, M.A., Post, A.F., Paytan, A., 2011. The influence of light on nitrogen cycling and the primary nitrite maximum in a seasonally stratified sea. Prog. Oceanogr. 91, 545–560. https://doi.org/10.1016/j.pocean.2011.09.001

Marañón, E., 2015. Cell Size as a Key Determinant of Phytoplankton Metabolism and Community Structure. Annu. Rev. Mar. Sci. 7, 241–264. https://doi.org/10.1146/annurev-marine-010814-015955

Marañón, E., Behrenfeld, M.J., González, N., Mouriño, B., Zubkov, M.V., 2003. High variability of primary production in oligotrophic waters of the Atlantic Ocean: uncoupling from phytoplankton biomass and size structure. Mar. Ecol. Prog. Ser. 257, 1–11. https://doi.org/10/dqhww3

Marañón, E., Holligan, P.M., Varela, M., Mouriño, B., Bale, A.J., 2000. Basin-scale variability of phytoplankton biomass, production and growth in the Atlantic Ocean. Deep Sea Res. Part Oceanogr. Res. Pap. 47, 825–857. https://doi.org/10/fq6vc9

Meeder, E., Mackey, K.R.M., Paytan, A., Shaked, Y., Iluz, D., Stambler, N., Rivlin, T., Post, A.F., Lazar, B., 2012. Nitrite dynamics in the open ocean—clues from

seasonal and diurnal variations. Mar. Ecol. Prog. Ser. 453, 11–26. https://doi.org/10/df98vc

Melo, P.A.M.C., Diaz, X.F.G., Macedo, S.J., Neumann-Leitão, S., 2012. Diurnal and spatial variation of the mesozooplankton community in the Saint Peter and Saint Paul Archipelago, Equatorial Atlantic. Mar. Biodivers. Rec. 5, 1–14. https://doi.org/10/ggczfq

Mena, C., Reglero, P., Hidalgo, M., Sintes, E., Santiago, R., Martín, M., Moyà, G., Balbín, R., 2019. Phytoplankton Community Structure Is Driven by Stratification in the Oligotrophic Mediterranean Sea. Front. Microbiol. 10. https://doi.org/10/gg9cwb

Metzler, P.M., Glibert, P.M., Gaeta, S.A., Ludlam, J.M., 1997. New and regenerated production in the South Atlantic off Brazil. Deep Sea Res1 Ocean. 44, 363–384. https://doi.org/10/d4rpjd

Mignot, A., Claustre, H., Uitz, J., Poteau, A., D'Ortenzio, F., Xing, X., 2014. Understanding the seasonal dynamics of phytoplankton biomass and the deep chlorophyll maximum in oligotrophic environments: A Bio-Argo float investigation. Glob. Biogeochem. Cycles 28, 856–876. https://doi.org/10/f6j525

Mishra, R.K., Senga, Y., Nakata, K., Mishra, S., Sahu, B.K., 2020. Spatio-temporal variation of Prochlorococcus and phytoplankton community between Shimizu coast and Suruga bay, Northwest Pacific Ocean. Reg. Stud. Mar. Sci. 33, 100890. https://doi.org/10/gg3hsj

Mishra, R.K., Shaw, B.P., Sahu, B.K., Mishra, S., Senga, Y., 2009. Seasonal appearance of Chlorophyceae phytoplankton bloom by river discharge off Paradeep at Orissa Coast in the Bay of Bengal. Environ. Monit. Assess. 149, 261–273. https://doi.org/10/ffvwpq

Moore, L.R., Rocap, G., Chisholm, S.W., 1998. Physiology and molecular phylogeny of coexisting Prochlorococcus ecotypes. Nature 393, 464–467. https://doi.org/10.1038/30965

Otsuka, A.Y., Feitosa, F.A. do N., Montes, M. de J.F., Silva, A.C. da, 2018. Influence of fluvial discharge on the dynamics of Chlorophyll-α in the continental shelf adjacent to the Recife Port Basin (Pernambuco-Brazil). Braz. J. Oceanogr. 66, 91–103. https://doi.org/10.1590/s1679-87592018149106601

Paulo, J.G., 2016. Distribuição vertical dos nutrientes dissolvidos no Nordeste do Brasil entre as latitudes 6° 20'S e 7° 33'S. Universidade Federal de Pernambuco.

Pérez, V., Fernández, E., Marañón, E., Serret, P., Varela, R., Bode, A., Varela, M., Varela, M.M., Morán, X.A.G., Woodward, E.M.S., Kitidis, V., García-Soto, C., 2005. Latitudinal distribution of microbial plankton abundance, production, and respiration in the Equatorial Atlantic in autumn 2000. Deep Sea Res. Part Oceanogr. Res. Pap. 52, 861–880. https://doi.org/10/cp6csx

Qu, T., Meyers, G., 2005. Seasonal variation of barrier layer in the southeastern tropical Indian Ocean. J. Geophys. Res. Oceans 110. https://doi.org/10/cbcw8p

Queiroz, A.R., Flores Montes, M., Melo, P.A.M.C., Silva, R.A., Koening, M.L., 2015. Vertical and horizontal distribution of phytoplankton around an oceanic archipelago of the Equatorial Atlantic. Mar. Biodivers. Rec. 8, 1–13. https://doi.org/10/gf7kmv

Rii, Y.M., Karl, D.M., Church, M.J., 2016. Temporal and vertical variability in picophytoplankton primary productivity in the North Pacific Subtropical Gyre. Mar. Ecol. Prog. Ser. 562, 1–18. https://doi.org/10.3354/meps11954

Roy, S., Llewellyn, C.A., Egeland, E.S., Johnsen, G., 2011. Phytoplankton Pigments: Characterization, Chemotaxonomy and Applications in Oceanography. Cambridge University Press.

Ryabov, A.B., Rudolf, L., Blasius, B., 2010. Vertical distribution and composition of phytoplankton under the influence of an upper mixed layer. J. Theor. Biol. 263, 120–133. https://doi.org/10/fr7hjm

Sherr, E.B., Sherr, B.F., 2007. Heterotrophic dinoflagellates: a significant component of microzooplankton biomass and major grazers of diatoms in the sea. Mar. Ecol. Prog. Ser. 352, 187–197. https://doi.org/10/d8s5p6

Signorini, S.R., Franz, B.A., McClain, C.R., 2015. Chlorophyll variability in the oligotrophic gyres: mechanisms, seasonality and trends. Front. Mar. Sci. 2. https://doi.org/10/gg7tj2

Souza, C.S., Luz, J.A.G., Macedo, S., Montes, M. de J.F., Mafalda, P., 2013. Chlorophyll *a* and nutrient distribution around seamounts and islands of the tropical south-western Atlantic. Mar. Freshw. Res. 64, 168–184. https://doi.org/10/f4qx95

Stramma, L., England, M., 1999. On the water masses and mean circulation of the South Atlantic Ocean. J. Geophys. Res. Oceans 104, 20863–20883. https://doi.org/10/bvxhdz

Tchamabi, C.C., Araujo, M., Silva, M., Bourlès, B., 2017. A study of the Brazilian Fernando de Noronha island and Rocas atoll wakes in the tropical Atlantic. Ocean Model. 111, 9–18. https://doi.org/10/f92mvn

Toseland, A., Daines, S.J., Clark, J.R., Kirkham, A., Strauss, J., Uhlig, C., Lenton, T.M., Valentin, K., Pearson, G.A., Moulton, V., Mock, T., 2013. The impact of temperature on marine phytoplankton resource allocation and metabolism. Nat. Clim. Change 3, 979–984. https://doi.org/10/f5p2g3

Travassos, P., Hazin, F., Zagaglia, J., Advíncula, R., 1997. Estrutura Termohalina da Zona Econômica Exclusiva (ZEE) do Nordeste brasileiro durante a Expedição Oceanográfica JOPS II do NOc. Victor Hensen-Influências das Ilhas e Bancos oceânicos. Presented at the Congresso Latino Americano de Ciências Sobre o Mar, p. 502.

Vargas, C.A., Martínez, R.A., Cuevas, L.A., Pavez, M.A., Cartes, C., GonzÁlez, H.E., Escribano, R., Daneri, G., 2007. The relative importance of microbial and classical food webs in a highly productive coastal upwelling area. Limnol. Oceanogr. 52, 1495–1510. https://doi.org/10/frznhv

Vrede, T., Ballantyne, A., Mille-Lindblom, C., Algesten, G., Gudasz, C., Lindahl, S., Brunberg, A.K., 2009. Effects of N: P loading ratios on phytoplankton community composition, primary production and N fixation in a eutrophic lake. Freshw. Biol. 54, 331–344. https://doi.org/10.1111/j.1365-2427.2008.02118.x

Weinbauer, M.G., 2004. Ecology of prokaryotic viruses. FEMS Microbiol. Rev. 28, 127–181. https://doi.org/10.1016/j.femsre.2003.08.001

Wood, S.N., 2006. On Confidence Intervals for Generalized Additive Models Based on Penalized Regression Splines. Australian & New Zealand Journal of Statistics 48, 445–464. https://doi.org/10.1111/j.1467-842X.2006.00450.x

Wood, S.N., 2011. Fast stable restricted maximum likelihood and marginal likelihood estimation of semiparametric generalized linear models. J. R. Stat. Soc. Ser. B Stat. Methodol. 73, 3–36. https://doi.org/10/cbb27p

Yasunaka, S., Kouketsu, S., Strutton, P.G., Sutton, A.J., Murata, A., Nakaoka, S., Nojiri, Y., 2019. Spatio-temporal variability of surface water pCO2 and nutrients in the tropical Pacific from 1981 to 2015. Deep Sea Res. Part II Top.

Stud. Oceanogr., Understanding changes in transitional areas of the Pacific Ocean 169–170, 104680. https://doi.org/10.1016/j.dsr2.2019.104680

Zapata, M., Fraga, S., Rodríguez, F., Garrido, J.L., 2012. Pigment-based chloroplast types in dinoflagellates. Mar. Ecol. Prog. Ser. 465, 33–52. https://doi.org/10.3354/meps09879

Declaration of interests

☒ The authors declare that they have no known competing financial interests or personal relationships that could have appeared to influence the work reported in this paper.

☐The authors declare the following financial interests/personal relationships which may be considered as potential competing interests:

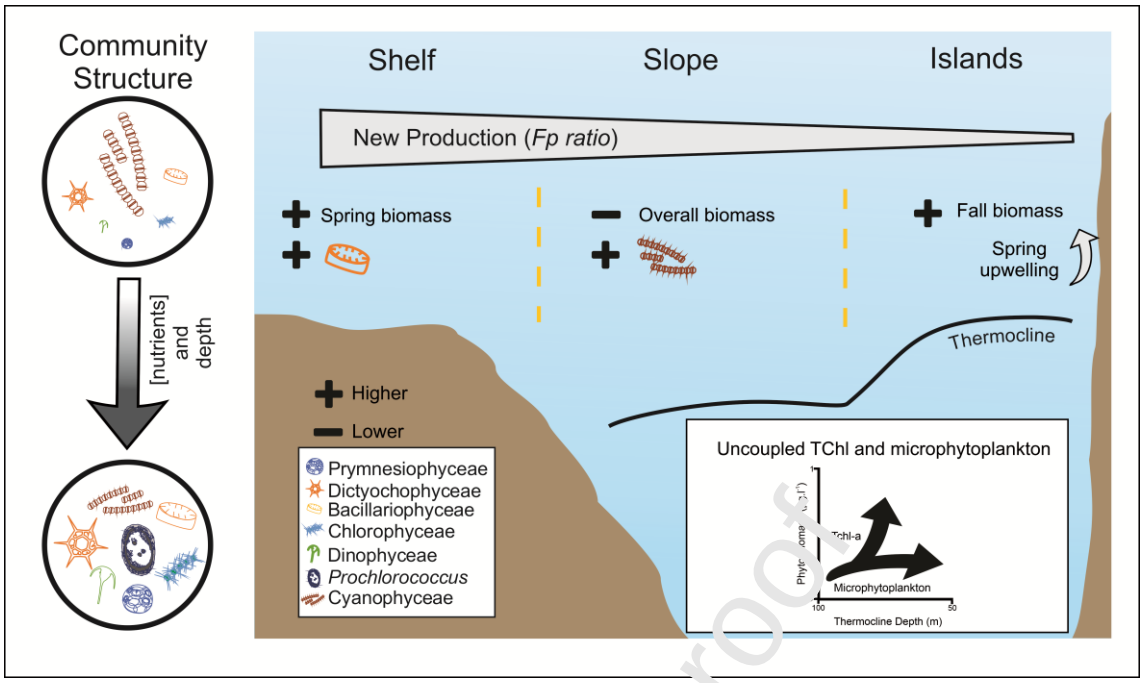

Uncoupled changes in phytoplankton biomass and size structure in the western tropical Atlantic

Highlights

- We unveiled uncoupled dynamics between phytoplankton size structure and biomass.
- A decreasing gradient of biomass and new production from shelf to offshore was pointed out.
- Seasonal changes in thermocline shape the phytoplankton dynamics and size structure.
- Phytoplankton diversity increased with depth but was mainly dominated by small cells.

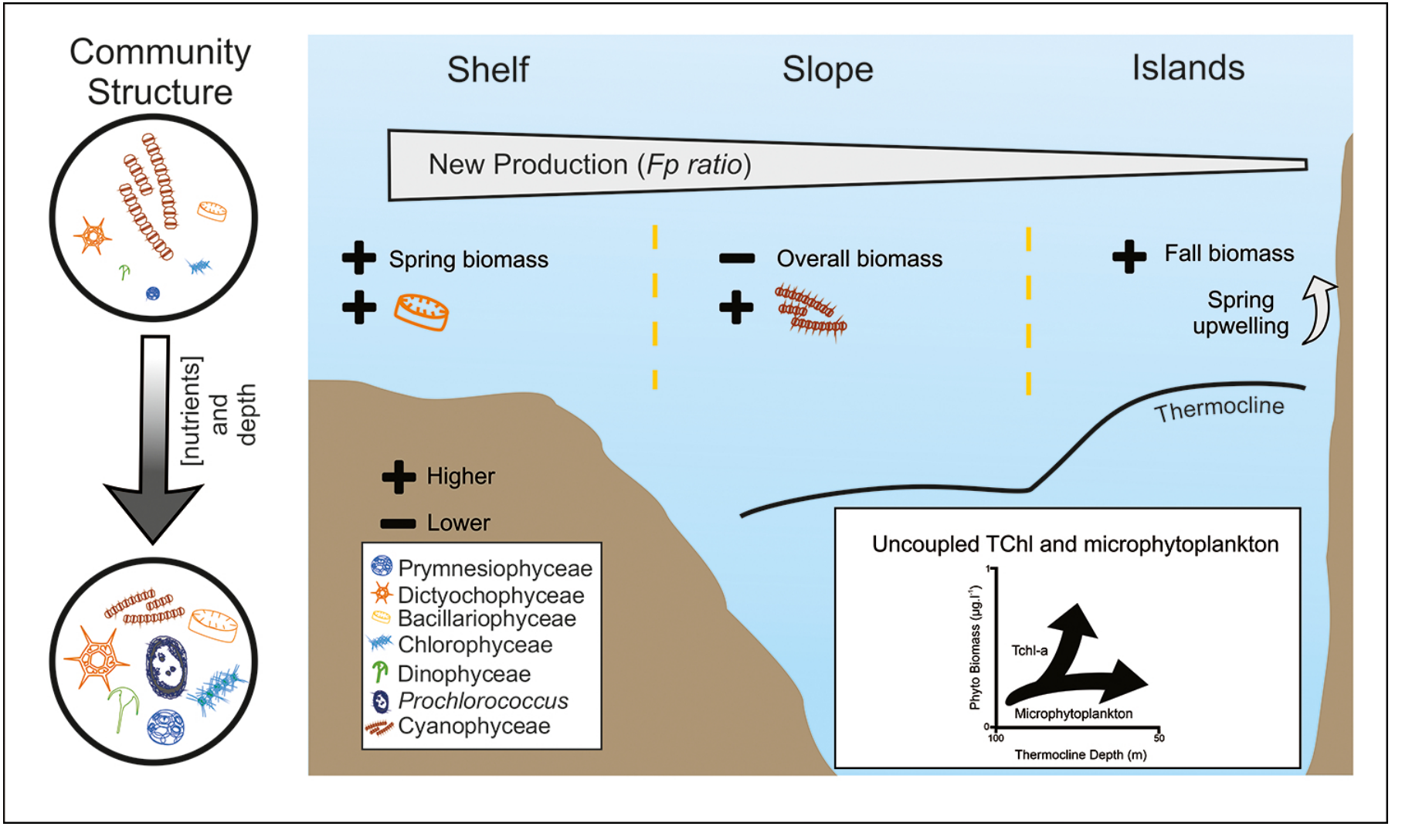

Graphics Abstract

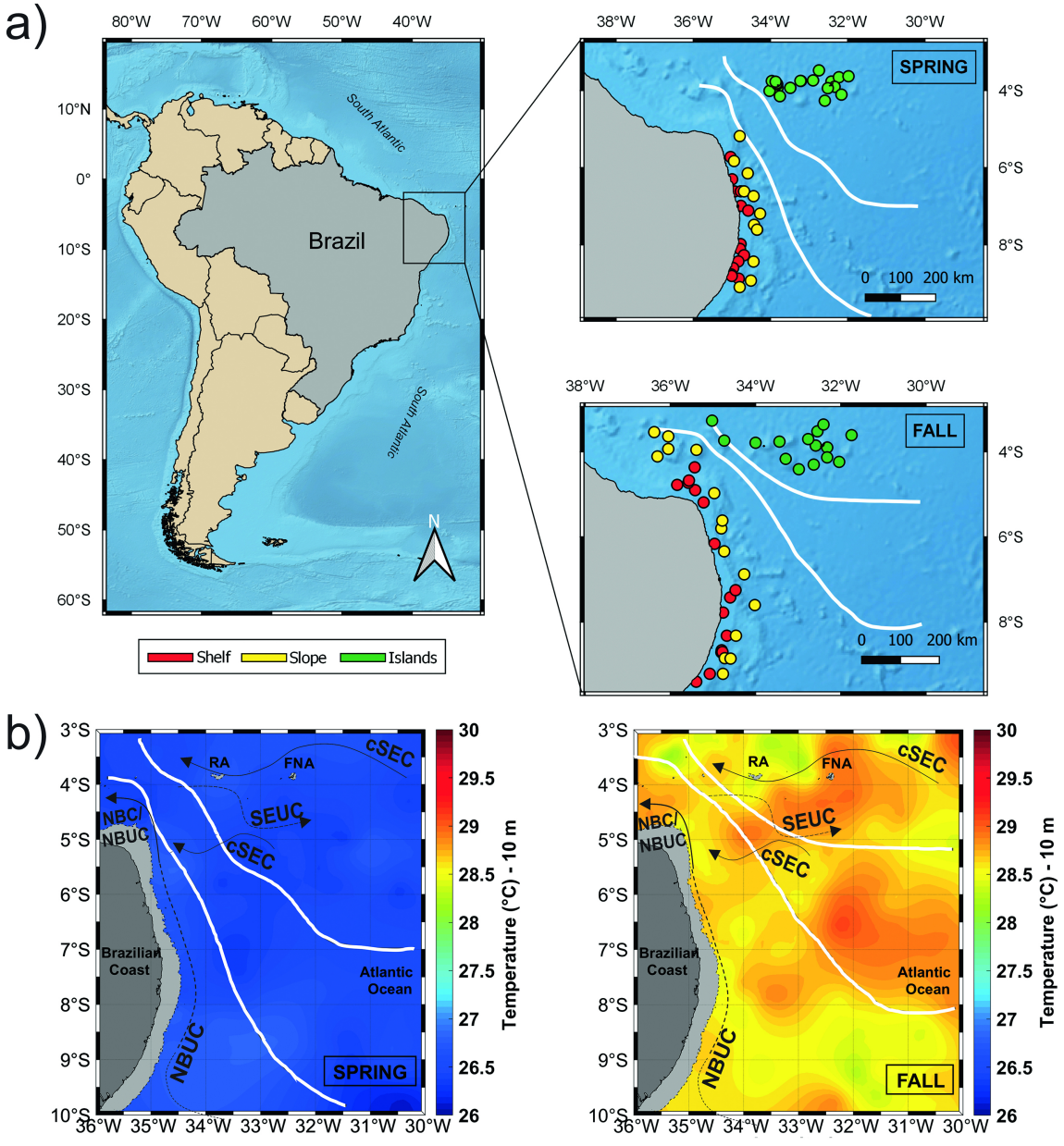
a)
80°W
70°W
60°W
50°W
40°W
10°N
0°
10°S
20°S
30°S
40°S
50°S
60°S
South Atlantic
Brazil
South Atlantic
N
Shelf
Slope
Islands
38°W
36°W
34°W
32°W
30°W
4°S
6°S
8°S
SPRING
0 100 200 km
FALL
0 100 200 km
b)
3°S
4°S
5°S
6°S
7°S
8°S
9°S
10°S
36°W
35°W
34°W
33°W
32°W
31°W
30°W
RA
FNA
CSEC
SEUC
NBC/
NBUC
Brazilian
Coast
Atlantic
Ocean
NBUC
SPRING
FALL
30
29.5
29
28.5
28
27.5
27
26.5
26
Temperature (°C) - 10 m

Figure 1

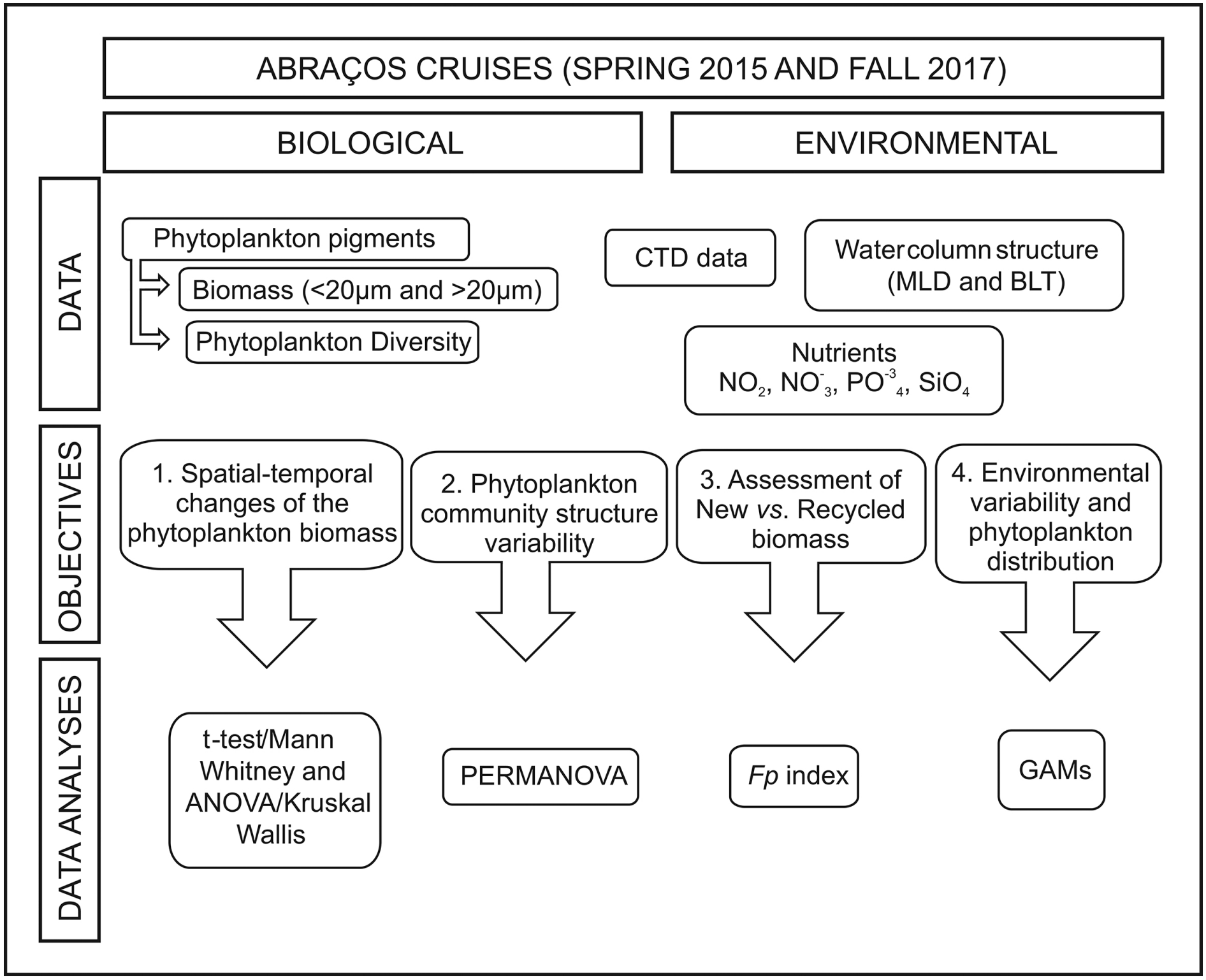
ABRAÇOS CRUISES (SPRING 2015 AND FALL 2017)
BIOLOGICAL
ENVIRONMENTAL
DATA
Phytoplankton pigments
Biomass (<20μm and >20μm)
Phytoplankton Diversity
CTD data
Water column structure (MLD and BLT)
Nutrients
NO_2, NO^-_3, PO^{-3}_4, SiO_4
OBJECTIVES
1. Spatial-temporal changes of the phytoplankton biomass
2. Phytoplankton community structure variability
3. Assessment of New *vs*. Recycled biomass
4. Environmental variability and phytoplankton distribution
DATA ANALYSES
t-test/Mann Whitney and ANOVA/Kruskal Wallis
PERMANOVA
Fp index
GAMs

Figure 2

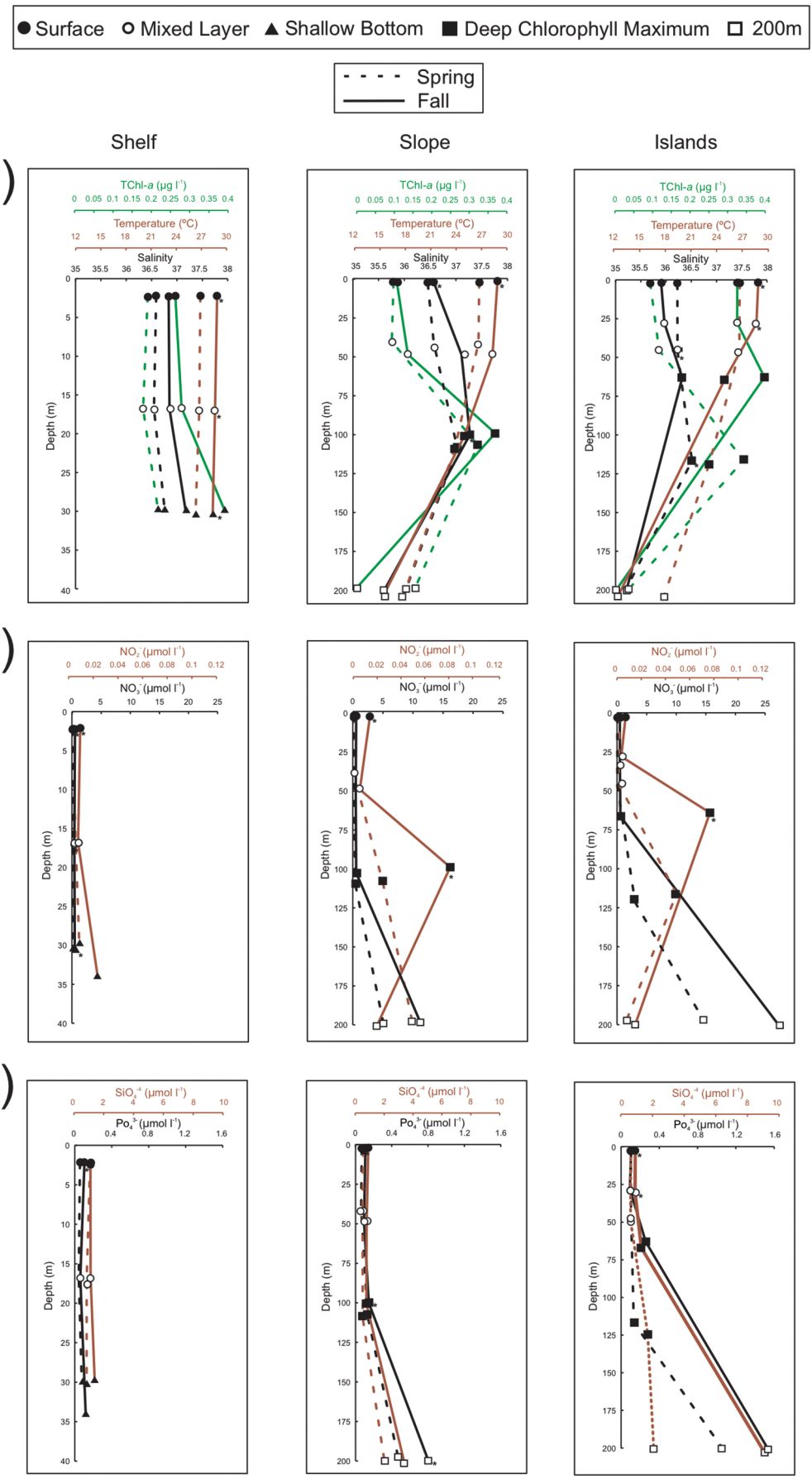
Surface
Mixed Layer
Shallow Bottom
Deep Chlorophyll Maximum
200m
Spring
Fall
Shelf
Slope
Islands
a)
b)
c)
TChl-a (µg l-1)
Temperature (ºC)
Salinity
NO2- (µmol l-1)
NO3- (µmol l-1)
SiO4-4 (µmol l-1)
Po4-3 (µmol l-1)
Depth (m)

Figure 3

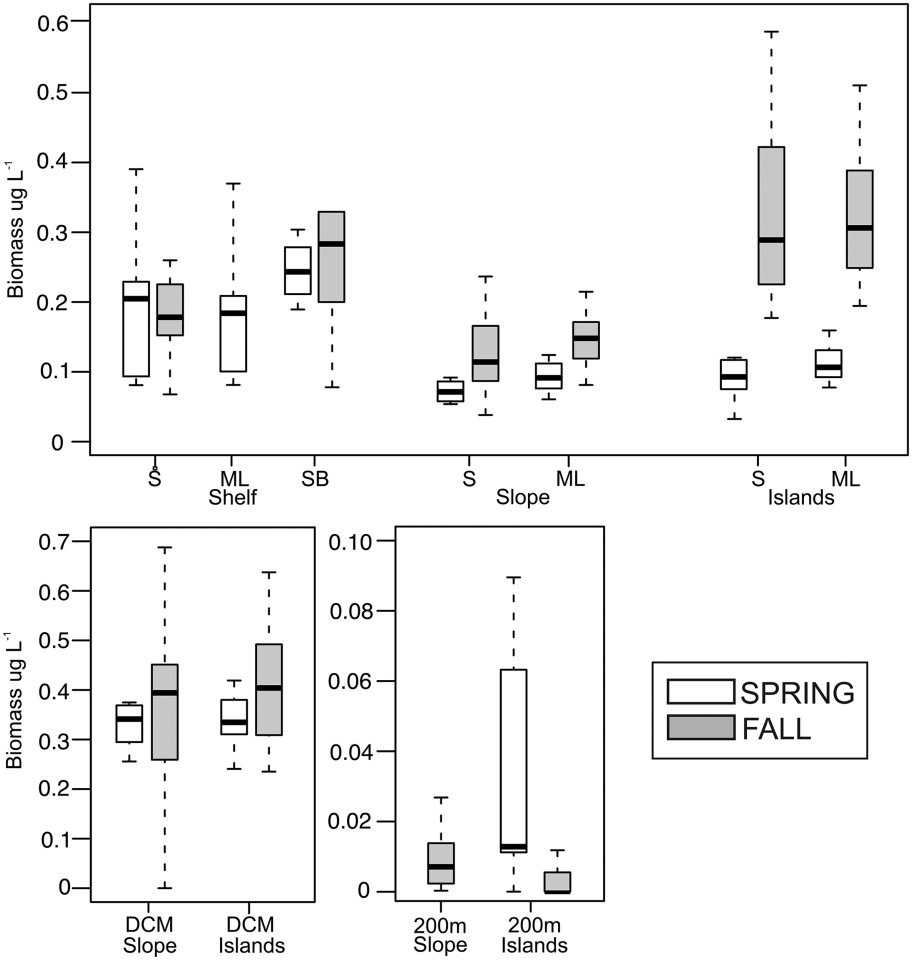
Biomass ug L-1
0.6
0.5
0.4
0.3
0.2
0.1
0
S
ML
SB
S
ML
S
ML
Shelf
Slope
Islands
Biomass ug L-1
0.7
0.6
0.5
0.4
0.3
0.2
0.1
0
0.10
0.08
0.06
0.04
0.02
0
DCM Slope
DCM Islands
200m Slope
200m Islands
SPRING
FALL

Figure 4

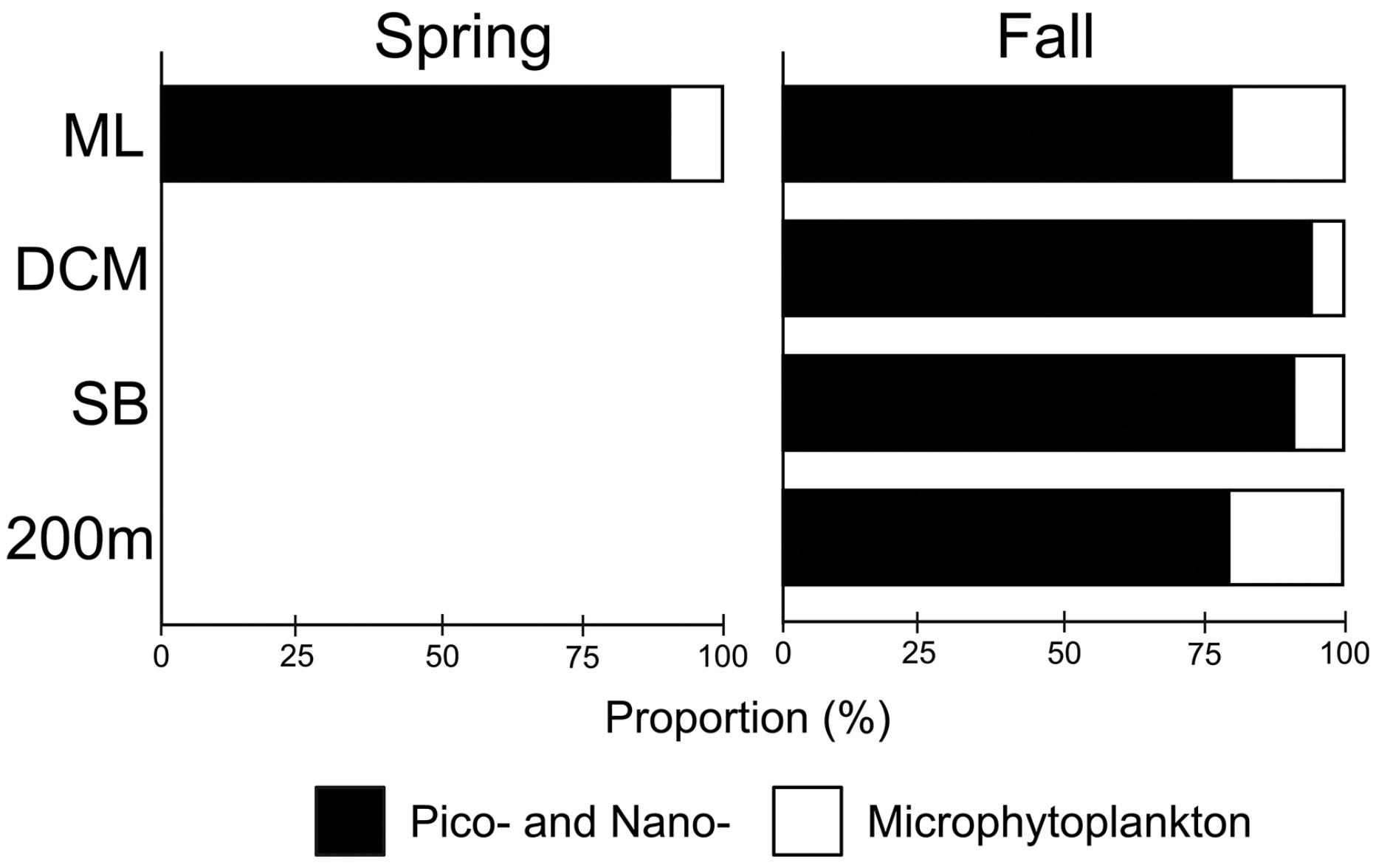
Spring
Fall
ML
DCM
SB
200m
0
25
50
75
100
0
25
50
75
100
Proportion (%)
Pico- and Nano-
Microphytoplankton

Figure 5

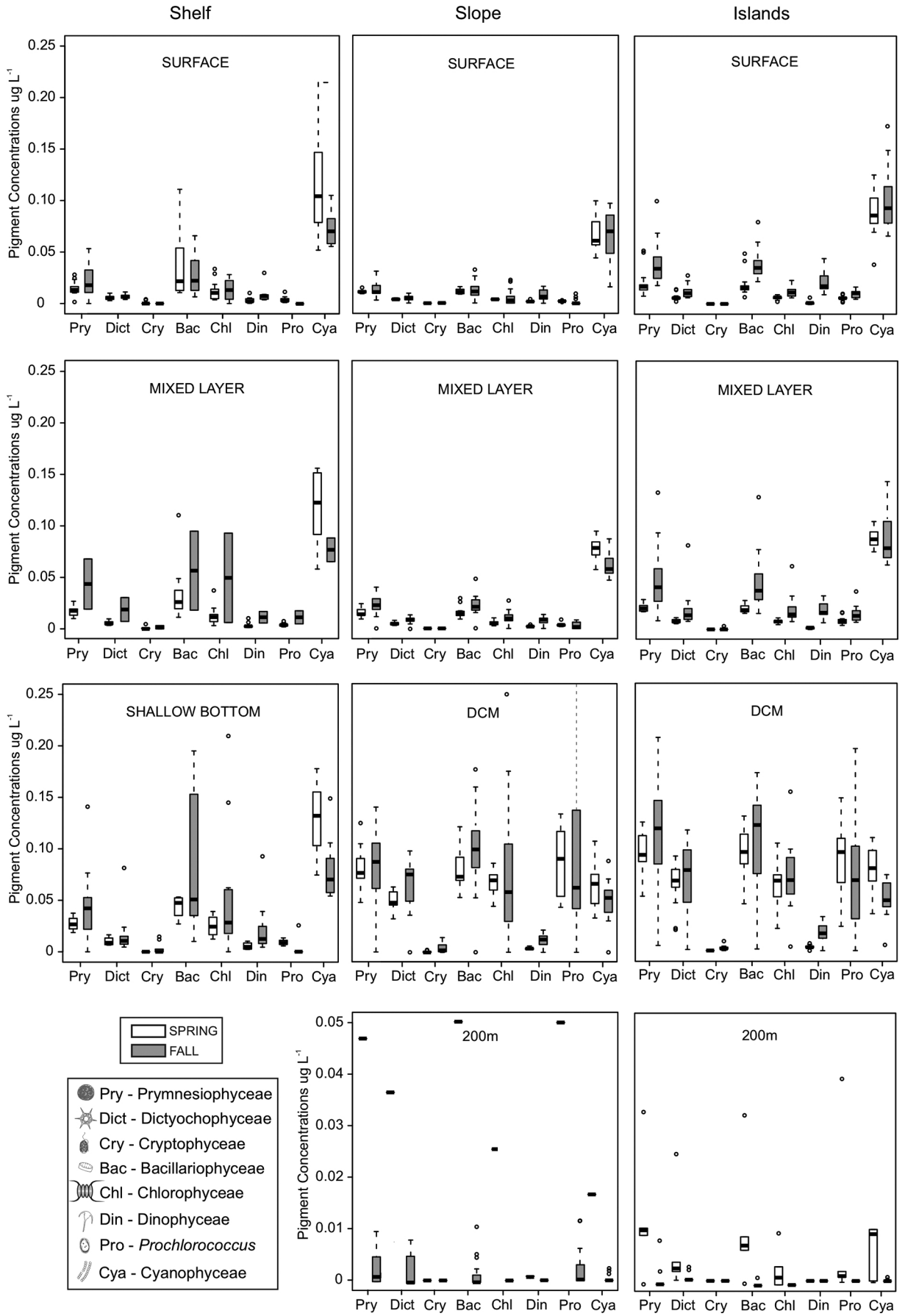
Shelf
Slope
Islands
SURFACE
MIXED LAYER
SHALLOW BOTTOM
DCM
200m
Pigment Concentrations ug L-1
0.25
0.20
0.15
0.10
0.05
0
Pry
Dict
Cry
Bac
Chl
Din
Pro
Cya
SPRING
FALL
Pry - Prymnesiophyceae
Dict - Dictyochophyceae
Cry - Cryptophyceae
Bac - Bacillariophyceae
Chl - Chlorophyceae
Din - Dinophyceae
Pro - Prochlorococcus
Cya - Cyanophyceae

Figure 6

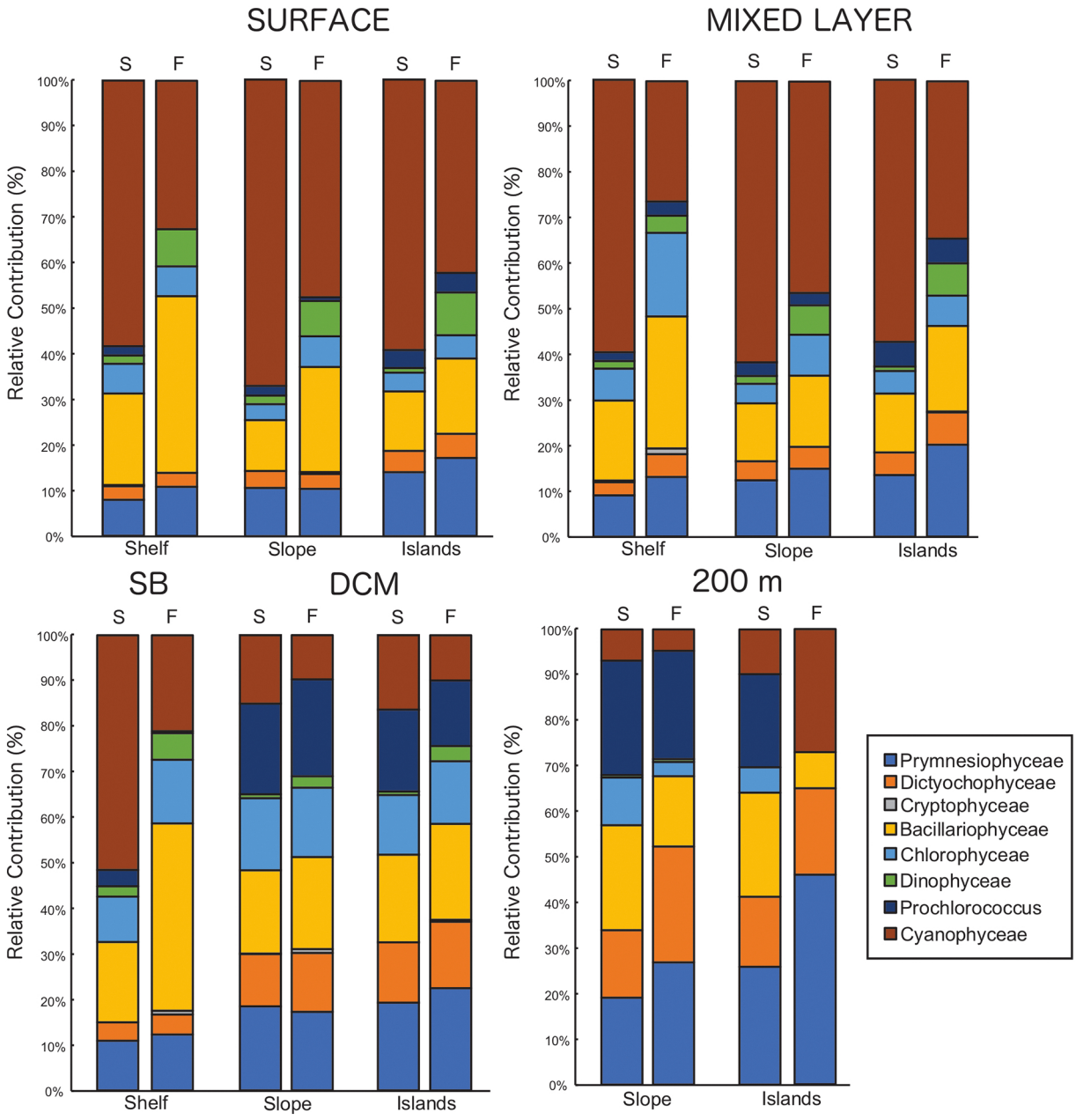
SURFACE
MIXED LAYER
SB
DCM
200 m
S
F
Relative Contribution (%)
100%
90%
80%
70%
60%
50%
40%
30%
20%
10%
0%
Shelf
Slope
Islands
Prymnesiophyceae
Dictyochophyceae
Cryptophyceae
Bacillariophyceae
Chlorophyceae
Dinophyceae
Prochlorococcus
Cyanophyceae

Figure 7

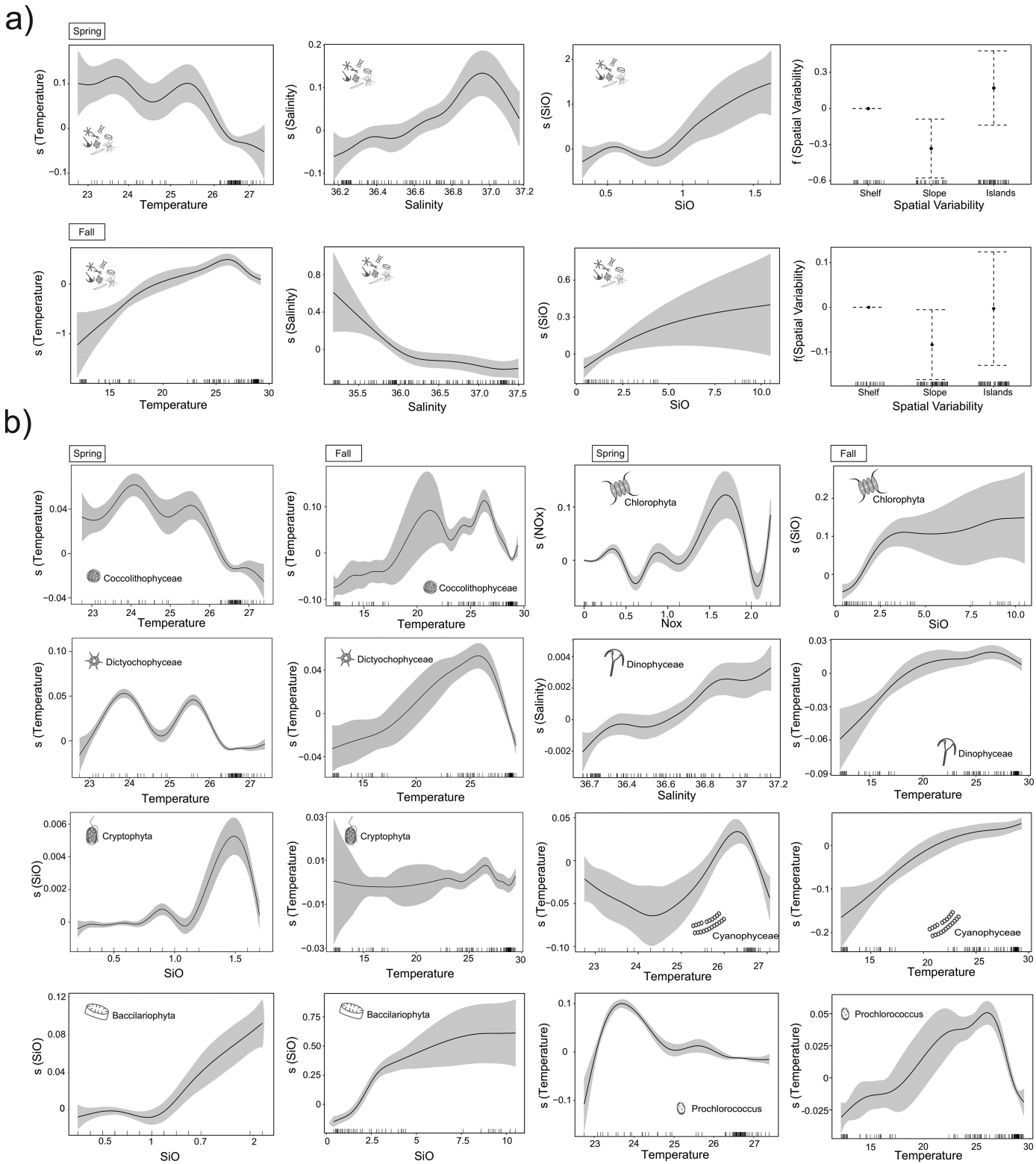
a)
Spring
s (Temperature)
Temperature
s (Salinity)
Salinity
s (SiO)
SiO
f (Spatial Variability)
Shelf
Slope
Islands
Spatial Variability
Fall
b)
Coccolithophyceae
Chlorophyta
s (NOx)
Nox
Dictyochophyceae
Dinophyceae
Cryptophyta
Cyanophyceae
Baccilariophyta
Prochlorococcus

Figure 8